Chapter 1: Introduction

Dear Reader of this Report,

this is the first annual report of our “Arbeitsgruppe Magnetismus“ (Laboratorium for Magnetism) at the Fachbereich Physik, Universität Kaiserslautern. Our group started in fall 1995 after I accepted the offer for a chair here in Kaiserslautern. After spending most of our time in 1995 and 1996 for setting up the labs, we achieved more or less “normal“ operating conditions in most of our labs in 1997 with first scientific results produced with the installed equipment. I feel that it is now timely to summarize our work in this Report. This first issue comprises the years 1996 and 1997.

A number of new experimental setups have been installed and put into operation in this year. The new multichamber molecular beam epitaxy (MBE) system has arrived. It allows the fabrication of epitaxial films and multilayers using two multipocket e^--beam evaporators and three Knudsen cells. Structural and chemical *in-situ* analysis is performed using Auger spectroscopy, low energy electron diffraction (LEED), reflected high energy electron diffraction (RHEED) and a scanning tunneling/atomic force microscope, which is prepared for operation as an *in-situ* magnetic force microscope. The system has a dedicated chamber for performing *in-situ* Brillouin light scattering and transverse Kerr-effect measurements in the temperature range 150 - 400 K at an applied field of up to ± 1.2 T. This instrument will allow for state-of-the-art investigations of surface magnetism phenomena under UHV-conditions with high-quality growth and structural characterization in the same system.

Our vibrating sample magnetometer is now working at room temperature, and the low temperature version is nearly completed. New in our lab is also a polar Kerr-effect magnetometer, which allows for measurements at fields of up to 5 T in the temperature range 2 - 400 K.

The installation of our clean room facility was completed and the laser interference lithography machine for patterning periodic structures in magnetic films was put into operation. We made first test structures (periodic wires and dot lattices) with periodicities down to 176 nm.

In the field of nonlinear spin wave propagation we opened a new experimental door by installing the option of time resolution to our scanning Brillouin light scattering setup. We can now study simultaneously the spatial distribution and the time evolution of microwave excited spin wave pulses.

The results of our work are summarized on the following pages. Highlights in 1997 were the discovery of a metastable Paladium bcc phase, the measurement of the spin wave quantization in narrow wires, the first time resolved Brillouin light scattering measurements of propagating spin wave pulses showing both transverse instability (self-focusing) and modulational instability, and the magnetic characterization of atomically layered Fe/Au multilayers.

Our work would not have been possible without valuable collaborations with groups over the world. I would like to thank Claude Chappert, Peter Grünberg, Gianluca Gubbiotti, Uwe Hartmann, Reiner Jungblut, Boris Kalinikos, Mikhail Kostylev, Stuart Parkin, Yuri Rapoport, Francoise Rousseaux, Hans Schmoranzer, Ivan Schuller, Andrei Slavin, Bob Stamps, and Stefan Visnovsky for their interactions with us and their strong input on our work. I would also like to thank all sponsors, which are the Deutsche Forschungsgemeinschaft, the Humboldt Foundation, the European Community, the State of Rheinland-Pfalz and the University of Kaiserslautern. My special thank is to Oliver Büttner, Kurt Jung, Sibylle Müller and Martin Rohmer for their technical help in preparing this Report.

If you like our work we would be happy to hear about it from you. If you have any questions, comments, suggestions or any kind of criticism please contact us.

With all my best wishes for 1998,

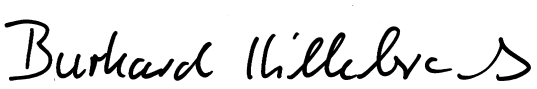

Kaiserslautern, December 1997

Chapter 2: Personnel

2.1 Members of the group

Group leader:

Prof. Dr. Burkard Hillebrands

Senior scientists:

Dr. Kurt Jung, Akad. Oberrat
Dr. Serguei Demokritov, Wiss. Assistent, since 9/95

PhD students:

Dipl.-Phys. Christoph Mathieu
Dipl.-Phys. Steffen Riedling
Dipl.-Phys. André Frank
Dipl.-Phys. Martin Bauer
Dipl.-Phys. Oliver Büttner

Diploma students:

Andreas Pletsch	until Oct. 96
Birgit Vogelgesang	until April 97
Claudia Hartmann	until June 97
Björn Roos	
Volker Wiehn	
Peter Kimmel	
Calin Radu	
Nikolaus Knorr	
Martin Rohmer	
Jörg Jorzick	
Patrick Cortina	
Uwe Schuth	
Marc Rickert	

Technician:

Bernd Pfaff

Secretary:

Sibylle Müller

2.2 Guests of the group

Carla Byloos	01.07.96-30.06.97
Honoré de Gronckel	01.02.96-30.04.96
Gianluca Gubbiotti	15.09.97-30.11.97
Michael Kostylev	22.09.97-31.10.97
Andrei Slavin	25.06.97-29.06.97
Yun-Jun Tang	01.10.97-30.09.98

Carla Byloos

Country: Italy
Visiting period : July '96 to June '97

My stay in Kaiserslautern was supported by the University of Ferrara with a grant for improving research skills abroad.

I chose the University of Kaiserslautern because of an established old collaboration between Prof. Hillebrands and Prof. Nizzoli (the supervisor of my degree thesis in Ferrara). The subject of the work was the determination of the dispersion relation of surface acoustic waves (in particular of Rayleigh waves) in a supported periodically composed film. The aim was to use these results for the determination of the relative Brillouin cross section and to compare them with the experimental data obtained for samples produced and measured in Kaiserslautern. The calculation of surface waves velocities should be done by a Fortran program in which the basic acoustic wave equations in term of their Fourier components were implemented. The program is now working for a periodic semi-infinite medium and the part regarding the film will be implemented in future.

Gianluca Gubbiotti

Country: Italy
Visiting period: 15.9.97 to 30.11.97

My name is Gianluca Gubbiotti and I am at the second year of my PhD in Materials Science. I come from the University of Perugia (Italy) where I work in an experimental group whose research activity is now mainly devoted to the study of magnetic properties of ultrathin films and multilayers. In particular, during the last year, we have applied the Brillouin light scattering technique to investigate the magnetic properties of ultrathin (111)-oriented Ni films where an appreciable in-plane directional dependence of the spin-wave frequency has been observed.

In order to interpret out experimental data we have extended to the case of a (111)-oriented cubic crystal a theoretical model previously proposed by Professor Hillebrands for an in-plane magnetized film. Therefore one of the reasons for my visit here in Kaiserslautern is to discuss this model for the spin-wave frequency calculation.

Concerning the experimental aspects, I would like to gain much experience on the magnetic properties of two-dimensional systems such as: ultrathin and wedged films, magnetic dots and wires. In

addition, I would also like to take part in the *in situ* Brillouin measurements and to learn the improvements which are necessary when BLS is applied for UHV measurements. This could be very useful for me since we are planning to set up in Perugia a similar UHV system for sample preparation and *in situ* Brillouin characterization of magnetic monolayers through detection of spin waves.

Dr. Mikhail Kostylev

Country: Russia
Visiting period: 19.9.97 to 30.10.97

My name is Mikhail Kostylev and I am a research fellow at the St. Petersburg Electrotechnical University (St. Petersburg, Russia). I belong to the research group of Prof. B. Kalinikos, and our research activity is mainly devoted to the investigation of nonlinear spin wave processes in magnetic films. My stay with Prof. Dr. Burkard Hillebrands' group was funded by the Deutsche Forschungsgemeinschaft under a research project dedicated to the investigation of nonlinear spin-wave phenomena. Five partners take part in this international project. From the german side, beside the Prof. Hillebrands' group, the groups of Priv.-Doz. Hartmut Benner at the Technische Universität Darmstadt (former Technische Hochschule Darmstadt), of Prof. H. Dötsch at the University of Osnabrück, and that of Prof. Josef Pelzl at the Ruhr-Universität Bochum are also involved.

During my 6-week stay at the University of Kaiserslautern in September-October 1997 I was making some numerical calculations concerning the theoretical explanation of experimental data on observation of propagation of nonlinear spin waves and nonlinear spin-wave packets in magnetic films. These data were obtained here in Kaiserslautern by using the Brillouin light scattering technique [1] as well as at the St. Petersburg Electrotechnical University [2] and at the Colorado State University (Prof. Patton's research group) by using a microwave measurement technique [3]. The first part of my work here was dedicated to a numeric modelling of spin-wave soliton propagation in magnetic films under parallel pump. A computer program was developed based on an earlier constructed formalism. Calculations were made by using the program. The calculations explained partly the previously obtained experimental data on the spin-wave soliton parametric amplification [2,3]. But the calculations showed also that additional experimental and theoretical investigations should be made in order to explain the phenomenon properly.

From this point of view the experimental data on the Brillouin light scattering (BLS) from nonlinear and parametric spin waves in YIG-film waveguides obtained in the Prof. Hillebrands' group are very helpful for me [1]. The experiments showed that backward volume spin waves in YIG films are very unstable under perturbations of transverse distributions of the dynamic magnetization. Hence the transverse modulational instability of the waves of this type, which in this particular case led to a nonlinear spin-wave width-mode coupling, should be always accounted for. This may be one of the possible causes of the discrepancies between the theory and the experiment on the spin wave soliton parametric amplification. In order to explain the nonlinear spin wave coupling some calculations were made by me based on the model of the nonlinear parabolic equation. The results of the calculations are in a better qualitative and quantitative agreement with the BLS experiment, than the earlier ones.

Another important research field at the University of Kaiserslautern is the direct observation of the parametrically excited spin waves in YIG films by using the BLS technique. The reasearch is only starting. A strongly inhomogeneous magnetic field of a microwave microstip transducer is used as a

source of the pump in the experiment. It was very interesting for me to take part in this research. In particular, because results of the research might be applied for explanation of the results of the experimental observation of „interaction“ of spin-wave envelope solitons with parallel pump field.

References:

[1] O.Büttner, M.Bauer, C.Mathieu, S.O.Demokritov, B.Hillebrands, P.A. Kolodin, M.P. Kostylev, S. Sure, H. Dötsch, V. Grimalsky, Yu. Rapoport, and A.N. Slavin, *Mode Beating of Spin Wave Beams in Ferrimagnetic* $LU_{2.04}Bi_{0.96}Fe_5O_{12}$ *Films*, submitted for publication in *IEEE Trans. on Magnetics.*

[2] B.A. Kalinikos, N.G. Kovshikov, M.P. Kostylev, P.A. Kabos, and C.E.Patton *Observation of Spin-Wave Soliton Amplification in Magnetic Films by Parallel Pumping*, submitted for publication in *JETP Letters.*

[3] P.A. Kolodin, P. Kabos, C.E. Patton, B.A. Kalinikos, N.G. Kovshikov and M.P. Kostylev *Amplification of Microwave Magnetic Envelope Solitons in Thin Yttrium Iron Garnet Films by Parallel Pumping*, submitted for publication in *Phys. Rev. Lett.*

Dr. Yun-Jun Tang

Country: China
Visiting period: Oct '97 to Oct '98

My name is Tang Yun-Jun. I am a research fellow from the State Key Laboratory for Magnetism, Institute of Physics, Chinese Academy of Sciences (CAS), Beijing, P. R. China. My stay in Prof. Dr. B. Hillebrands research group in Kaiserslautern University is supported by the Alexander von Humboldt-Stiftung for one year starting from Oct. 1, 1997.

I have learned German for four months in Mannheim before I came to Kaiserslautern. So I can speak and understand a little German. This would be very convenient for me to work and live in Kaiserslautern. But I think I should do a lot of things to improve my German.

My research interest is mainly on magnetostrictive materials and devices, GMR thin films and spin tunneling junctions.

In 1992 I obtained my Master Degree in the field of materials sciences on the studies of metals and structural ceramics. After I obtained my Ph.D. at the Institute of Physics (CAS) in 1995 for the studies of giant magnetostrictive materials, I began to do some research in GMR thin films and spin tunneling junctions. During this time I was selected as an Alexander von Humboldt-Stiftung fellow to do research in Prof. B.Hillebrands' research group on the study of spin tunneling junctions for one year.

I would like to learn more about the research ideas, experimental skills, as well as the equipment in Prof. Hillebrands' research group. And I also would like to learn more about the people, culture, ... of Germany. I hope my stay here would be benefit for me and the research group, and finally for establishing a good relationship between Institute of Physics (CAS) and Kaiserslautern University.

Chapter 3: Research Topics

Our scientific work concentrates mostly on problems in basic research, which emerge from applications of magnetic structures in data storage and sensor devices.

Our research subjects are:

1) Investigations of the growth and structure of thin magnetic epitaxial films and multilayers

To study magnetic phenomena with the necessary precision the preparation of samples with highest possible structural quality is mandatory. We achieve this by using molecular beam epitaxy (MBE) in which the standard *in-situ* methods for chemical and structure analysis are employed. This is Auger spectroscopy for chemical analysis, low and high energy electron diffraction (LEED, RHEED), and a combined in-situ scanning tunneling and atomic force microscope (STM/AFM).

2) Magnetic properties of ultrathin magnetic films and multilayers

Of central interest to us is the determination and the origin of all contributing magnetic anisotropies, of magnetic moments at interfaces, of coupling phenomena between magnetic films, and of the influence of atomic defects, steps, roughness and interdiffusion on the magnetic properties. To study the magnetic properties we perform *in-situ* Brillouin light scattering spectroscopy (BLS) and magneto-optic Kerr-magnetometry in the MBE system. *Ex-situ,* the samples are investigated using Brillouin light scattering, vector Kerr magnetometry, vibrating sample magnetometry (VSM), alternating gradient magnetometry (AGM), Kerr microscopy and magnetic transport.

3) Giant magnetoresistance and tunneling magnetoresistance sensors

We investigate transport phenomena based on the giant magnetroresistance effect and the magnetic tunneling effect with the aim to develop new magnetic sensors. In a dedicated project we put special emphasis on the development of new methods to improve the structural quality of the isolating tunneling layers.

4) Modification of magnetic properties in thin films by patterning

Patterning of magnetic films allows to generate materials with new magnetic properties, like magnetic dot or wire arrays. Such structures probably will play a dominant role in future data storage and sensor applications. We focus on the investigation of the basic magnetic properties of such structures. For patterning we use a UV-laser interference lithography machine. In the department we have access to electron beam lithography and photo lithography.

5) Nonlinear properties of microwave excited spin waves

Using Brillouin light scattering we measure the intensities of spin waves propagating in a magnetic film with spatial resolution. The spin waves are excited by microwaves using a stripe antenna or a cavity. Using a pulsed microwave source and a time-gate technique, measurements can be performed with time resolution. Central problems are the propagation of spin waves in

the linear and nonlinear intensity regimes, the formation of instabilities (e.g. self-focusing), the propagation of nonlinear excitations (solitons) and the generation of subharmonics (parametric excitation).

6) Elastic properties of hard, superhard and inhomogeneous films and multilayers

We prepare hard and superhard films and investigate the elastic properties using Brillouin light scattering. Research subjects are amorphous carbon (a-C:H and ta-C:H) and cubic boron nitride films, which are prepared using plasma beam deposition and unbalanced magnetron sputtering. The elastic constants are determined from the dispersion curves of surface and film phonons (Rayleigh and Sezawa modes). Our aim is to prepare hard and superhard films with minimized internal stresses.

Chapter 4: Equipment

A) Preparation and characterization of thin films and multilayers

1) multichamber molecular beam epitaxy system (Pink) comprising
   (a) deposition chamber (electron beam and Knudsen sources, RHEED, LEED, Auger)
   (b) scanning tunneling and atomic force microscopy chamber (Park, in-situ STM/AFM)
   (c) Brillouin light scattering and Kerr magnetometry chamber (magnetic field 1.2 T, temperature range 120 - 400 K)
   (d) load lock chamber
   (e) preparation chamber (optical coating, heating station 2300° C)
   (f) transfer chamber
2) two-chamber molecular beam epitaxy system
3) plasma beam deposition system
4) magnetron sputtering system
5) scanning tunneling and atomic force microscope (TopoMetrix)

B) Patterning of magnetic films

1) UV laser interference lithography setup
2) clean room facility with flow box, spin coater, etc.

C) Magnetic characterization

1) vibrating sample magnetometer (magnetic field 1.6 T, room temperature) with alternating gradient magnetometer option
2) vibrating sample magnetometer (magnetic field 5 T, temperature range 2 - 350 K) (under construction)
3) vector Kerr magnetometer (longitudinal and transverse Kerr effect, magnetic field 1.2 T, room temperature, automated sample positioning)
4) high field polar Kerr magnetometer (magnetic field 5 T, temperature range 2 - 350 K)
5) Kerr microscope
6) Brillouin light scattering spectrometer, computer controlled and fully automated (magnetic field 2.2 T, temperature range 2 - 400 K) with scanning option for spin wave intensity mapping
7) microwave setup (up to 32 GHz) comprising a network analyser, microwave amplifier, modulators and pulse generators
8) magnetotransport setup (magnetic field 1.5 T, temperature range 20 - 400 K)

Chapter 5: Transfer of Technology

We offer consultance and transfer of technology in the areas of thin film magnetism, magnetic film structures and devices, magnetic sensors, and in corresponding problems of metrology.

We are equipped to perform magnetic, transport, elastic and structural measurements of films and multilayer systems.

This is in detail:

- magnetometry (magnetic field up to 5 T, temperature range 2 - 400 K) using vibrating sample magnetometry, Kerr magnetometry, Brillouin light scattering spectroscopy
- test of homogeneity of magnetic parameters
- exchange stiffness constants in magnetic films
- magnetic anisotropies (out-of-plane and in-plane) with high spatial resolution
- magnetotransport properties (giant and tunneling magnetoresistance)
- elastic constants
- surface topography

Chapter 6: Research reports

6.1 Discovery of a metastabile bcc-Pd phase

B. Roos, A. Frank, S.O. Demokritov, and B. Hillebrands

The epitaxial growth and structure of layered systems containing 3d magnetic metals covered by nonmagnetic films have been intensively studied during the past years due to the important role these systems play both in basic and applied research. Fe/Pd multilayers are of particular importance because of an anomalously large Pauli susceptibility of the Pd-atoms. One can expect unusual magnetic properties of this system. In fact, a strong dependence of the surface anisotropy constants on the Pd-layer thickness were recently observed (see Sect. 6.2 of this Report). Therefore, the epitaxial growth of Fe(001)/Pd(001) double layers, in particular in the case of low Pd coverages, is of great interest.

The sample preparation was performed in a UHV system with a base pressure better than 10^{-10} mbar by means of molecular beam epitaxy. The chemical and crystallographic analysis of the surfaces has been performed by *in situ* Auger electron spectroscopy (AES) and low energy electron diffraction (LEED). The films were deposited onto 5mm×10mm GaAs(001) substrates, covered by a 150 nm thick fcc Ag(001)-buffer layer. The detailed description of the preparation procedure is published elsewhere [1]. The best Pd layers were grown onto bcc Fe(001) at a growth temperature of 300°C with a growth rate of 0.02 monolayers (ML) per second. The samples were capped with a Cr or Ag overlayer to prevent oxidation. Good coverage of the Fe layers by Pd at 300°C is attested by the exponential decay of the Fe Auger peak (47 eV) intensity with increasing Pd thickness [2]. The Fe film is nearly completely covered by Pd at $d_{Pd} \approx 2$ ML.

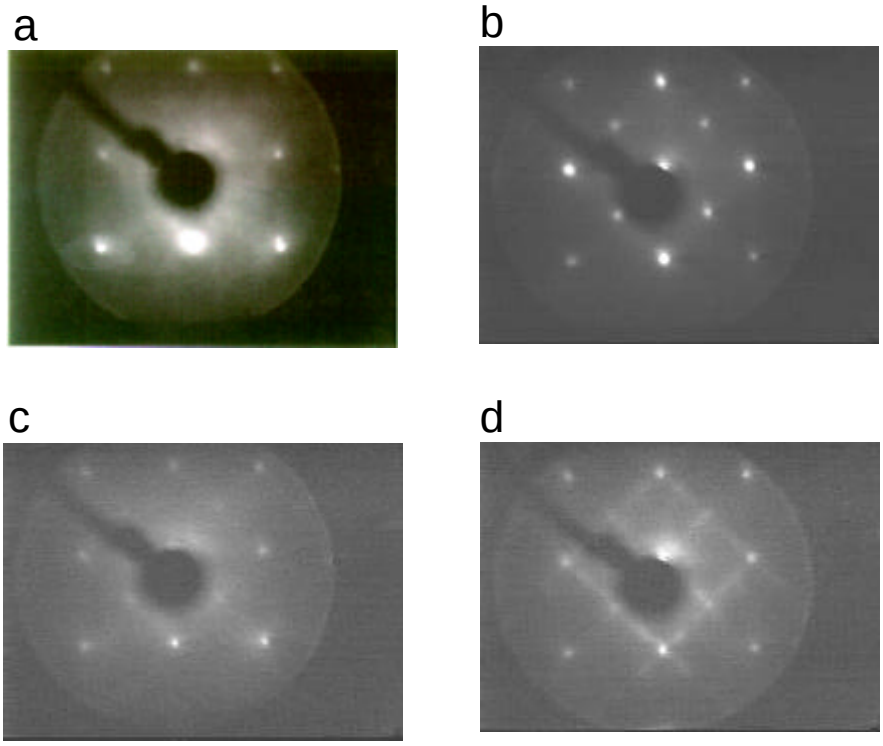

Fig. 1. LEED patterns at the successive growth steps of the Fe/Pd structure measured at an e-beam energy of 98 eV. **a)** Ag-buffer, **b)** 15ML Fe, **c)** 1.5ML Pd on Fe , **d)** 3ML Pd on Fe.

The LEED patterns observed during the preparation of a typical sample are shown in Fig. 1. The patterns of the Ag(001) buffer are almost ideal (Fig. 1a). The spots are very sharp and do not change in width with the beam energy. However, this is not the case for the LEED patterns of the as-deposited Fe film. Fig. 1b shows the LEED patterns of the Fe film annealed at 300°C during 300 s. After annealing the LEED patterns indicate a c(2×2)-reconstruction of the Fe(001) surface. Fig. 1c shows the LEED patterns for a 3ML-thick Pd film, grown on Fe, which is typical for Pd thicknesses between 2ML and 5 ML. It is indeed similar to the one of the Ag buffer and demonstrates the high-quality growth of Pd(001) on Fe(001). For thicker Pd films the LEED patterns deteriorate. As an example for the thin-film regime the LEED patterns of a 1.5ML thick Pd film are displayed in Fig. 1d. They show streaks connecting (01)- and (10)-spots, which can be attributed to a quasi-one-dimensional growth mode of Pd at such small coverages.

Our results (see also Sect. 6.2 of this Report) confirm that Pd overlayers strongly affect the magnetic anisotropy properties of Fe(001) films. It is surprising, that both the out-of-plane and the in-plane anisotropy contributions depend in a linear manner on d_{Pd} up to 5.5ML with suddenly following saturation. For a better understanding of this behaviour a detailed investigation of the Pd growth on Fe(001) was performed.

In terms of crystallographic registry both a Pd fcc and a bcc phase can exist on the Fe(001) surface, since both would have close nearest-neighbour distances within the (001)-plane. Since the bcc-(001)-plane contains one atom per unit cell, and the fcc(001)-plane contains two atoms, the fcc unit cell is rotated within the (001)-plane by 45° to achieve registry with the Fe(001) surface, wherease the Pd bcc-(001) unit cell is not rotated. The LEED patterns presented above do not allow to discriminate between both phases. It is likely that due to this reason a bcc phase was not considered in the literature so far. The difference between both phases lies in the perpendicular lattice spacing, which for the fcc phase is about a factor of $\sqrt{2}$ larger than for the bcc phase.

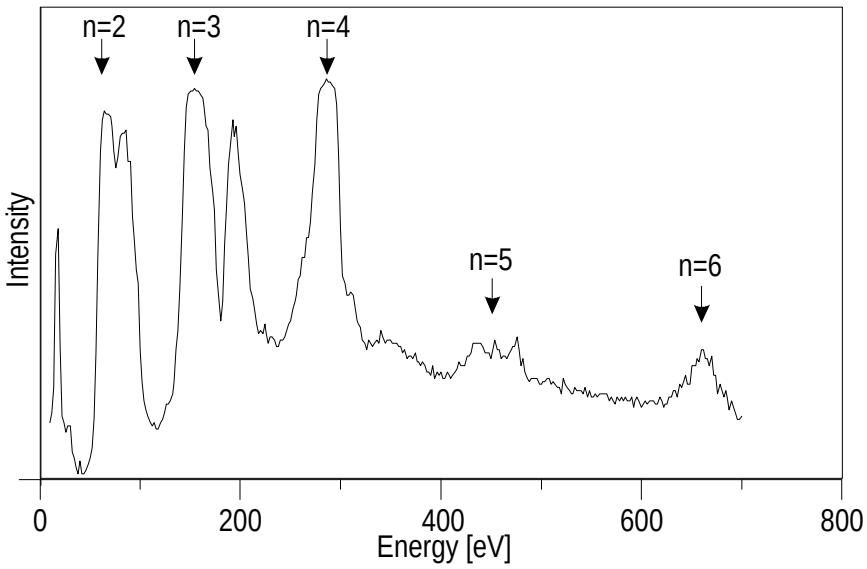

Fig. 2. The I(V)-curve of the (00)-spot, measured on Fe(001) surface. The arrows mark primary Bragg-reflexes.

To clarify the structure we have measured the perpendicular lattice spacing between the monolayers. This was performed by monitoring the LEED-I(V)-curves, which show the intensity of, for example, the (00)-spot versus the energy of the electron beam. Such curves are presented in Fig. 2 for different thicknesses of the Pd film. Maxima resulting from constructive interference of the electrons scattered by adjacent monolayers are clearly seen. From such curves the perpendicular lattice spacing between monolayers is derived. The results are shown in Fig. 3. It demonstrates that the dis-

tance between monolayers corresponds not to the fcc-Pd phase, but to the bcc-Pd phase. On the basis of this finding one can conclude, that the origin of the observed linear change of the anisotropy constants is a strain component in the Fe film caused by an substantially strained bcc-Pd layer, which is proportional to the Pd-thickness. At some critical thickness (our latest results show that this point depends drastically on the growth conditions) the isomorphic growth of Pd is destroyed and a polycrystalline Pd film is formed upon further growth. This polycrystalline Pd film is not strained and does not contribute to the strain of the Fe film.

A full report is in preparation [3].

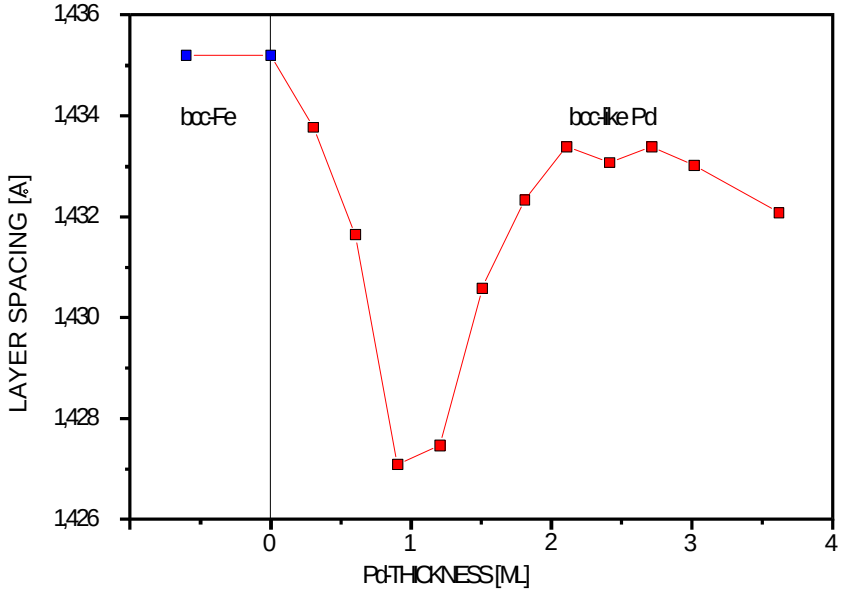

Fig. 3. The distance between monolayers as a function of the Pd-layer thickness, determined from the I(V)-curves.

References

[1] P. Grünberg, S. Demokritov, A. Fuss, R. Schreiber, J.A. Wolf, and S.T. Purcell, J. Magn. Mag. Mat. **104-107** 1734 (1992).
[2] G. Ertl, J. Küppers, "Low energy electrons and Surface Chemistry", VCH, Weinheim, p.7 (1985).
[3] B. Roos, A. Frank, S.O. Demokritov, B. Hillebrands, to be published.

6.2 Pd induced anisotropies in the Fe(001)/Pd bilayer system

C. Mathieu, M. Bauer, S. Riedling, O. Büttner, S.O. Demokritov, and B. Hillebrands

Since the last few years interface anisotropies have been investigated in many systems containing 3d magnetic metals covered by nonmagnetic films. The unique properties of Pd make the Fe/Pd system especially interesting. The free Pd atom has a $4d^{10}5s^2$ configuration and is nonmagnetic. However, in metallic Pd the 4d band is not entirely filled and it is nearly ferromagnetic with an anomalously large Pauli susceptibility. Therefore, one can expect that the magnetic properties of the Pd layers can be modified on ferromagnetic substrates, and, in turn, that the magnetic properties of the substrate are changed as well. In this Report we examine in detail the in-plane and out-of-plane Fe/Pd interface anisotropy contributions as a function of the Pd layer thickness and we compare these results with coercive field measurements.The sample preparation was performed in a UHV system with a base pressure better than 10^{-10} mbar by means of molecular beam epitaxy. The chemical and crystallographic analysis of the surfaces has been performed by *in situ* Auger electron spectroscopy (AES) and low energy electron diffraction (LEED). The films were deposited onto 5mm×10mm GaAs(001) substrates, covered by a 150 nm thick fcc Ag(001)-buffer layer. The best Pd layers were grown on Fe(001) at a growth temperature of 300°C with a growth rate of 0.02 monolayers (ML) per second. Good coverage of the Fe layers by Pd at 300°C is attested to by the exponential decay of the Fe Auger peak (47 eV) intensity with increasing Pd thickness. The Fe film are nearly completely covered by Pd at $d_{Pd} \approx 2$ ML.

The magnetic properties of the Fe/Pd double layers were investigated at room temperatures by Brillouin light scattering (BLS) from thermally excited spin waves and by magneto-optic Kerr effect (MOKE) magnetometry. All samples were found to be in-plane magnetized. From the measured spin waves frequencies all anisotropy contributions are obtained using an appropriate model. The external field H was always applied in the plane of the films. For MOKE measurements it was aligned along the easy in-plane axis.

Fig. 1 clearly demonstrates, that the four-fold symmetry of Fe films is not broken by the Pd overlayer. Therefore we write the anisotropy contribution to the free energy density as:

$$f_{an} = -K_{out} \cdot \cos^2 \theta + K_{in} \cdot \sin^4 \theta \cdot \cos^2 \varphi \cdot \sin^2 \varphi \qquad (1)$$

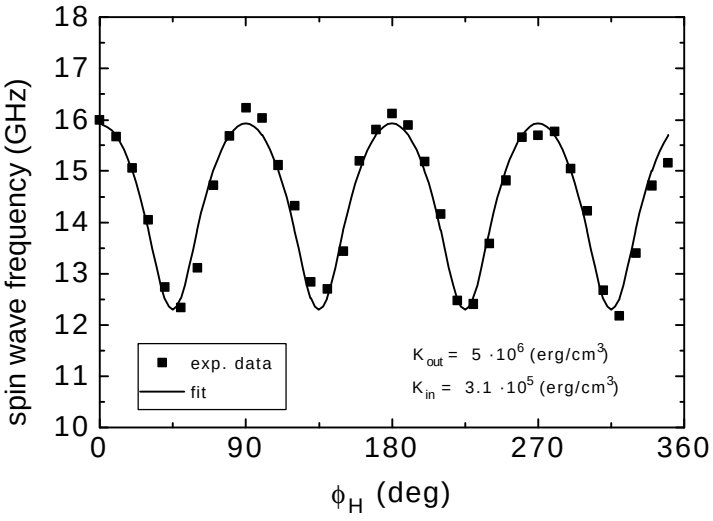

Fig. 1. Spin wave frequency for the 15ML Fe/1.5ML Pd sample, measured at H=1 kOe as a function of the in-plane angle ϕ_H between the field and the Fe-[100]-direction. The fit is performed on the basis of Eq. (1).

where θ is the polar angle of the direction of magnetization measured against the interface normal and φ is the azimuthal angle measured with respect to the [100] axis of Fe in the film plane. K_{out} and K_{in} are the out-of-plane and the in-plane anisotropy constants, respectively.

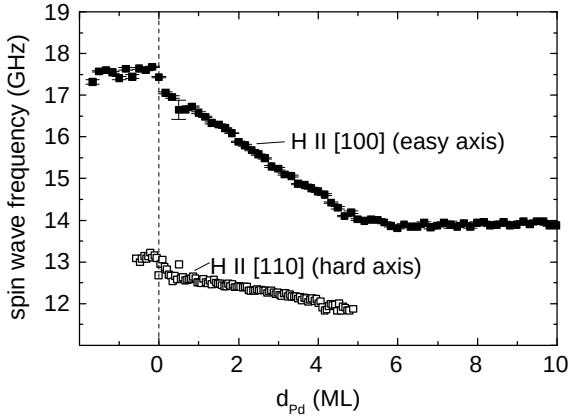

Fig.2. Spin wave frequency for a Pd wedge on a 15 ML thick Fe film, measured at H=1 kOe (þ : H along the easy [100]-direction, ÿ: H along the hard [110]-direction) as a function of d_{Pd}. d_{Pd}<0 corresponds to the uncovered Fe film and is used as a reference.

It is clear from Fig. 2, that the Pd deposition dramatically changes the spin wave frequencies even after the Fe-surface is completely covered by the Pd-layers for d_{Pd}>2 ML. Using a standard fit procedure [1], both K_{out} and K_{in} are determined from the experimental data. The results are shown in Fig. 3.

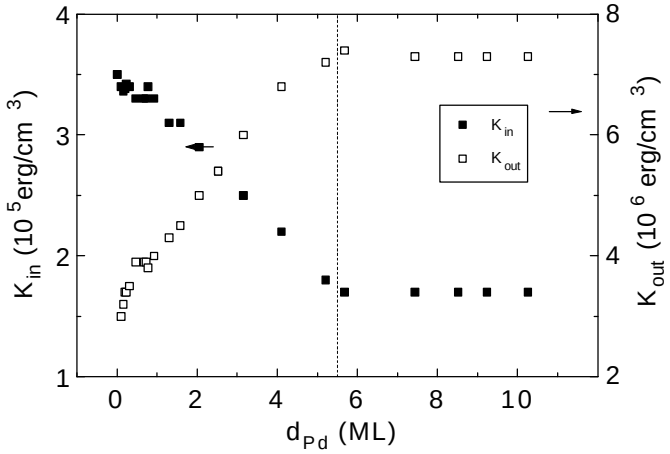

Fig. 3. Obtained anisotropy constants K_{in} and K_{out} for a Pd wedge on a 15 ML thick Fe film as a function of d_{Pd}.

The derived anisotropy constants, K_{out} and K_{in}, show a strong linear change with increasing d_{Pd} up to 5.5 ML with following saturation, with K_{out} showing an additional abrupt change in slope within the first monolayer of Pd coverage. Assuming that the Pd overlayer does not influence the bulk properties of the Fe films one can calculate the surface anisotropy contributions, their maximum changes being Δk_{out} = 0.8 erg/cm^2 and Δk_{in} = 0.04 erg/cm^2.

Our BLS and MOKE results confirm that Pd overlayers strongly affect the anisotropy properties of Fe(001) films. It is surprising, that both K_{out} and K_{in} depend on d_{Pd} up to 5.5ML and in a linear way. The origin is traced back to the growth of bcc-Pd up to 5.5ML (see Sec. 6.1).

A full report is published in [2].

References

[1] B. Hillebrands, Phys. Rev. B **41**, 530 (1990).
[2] S.O. Demokritov, C. Mathieu, M. Bauer, S. Riedling, O. Büttner and B. Hillebrands, J. Appl. Phys. **81**, 446 (1997).

6.3 Interlayer coupling and the giant magnetoresistance effect in Fe/Cr/Pd/Fe multilayers

C. Radu, S.O. Demokritov, and B. Hillebrands

Interlayer coupling and magnetotransport properties of various magnetic multilayers have been investigated intensively over the past decade. Many pioneering studies have been performed on Fe/Cr multilayers during this time. The Fe/Cr system shows both a strong antiferromagnetic coupling and the giant magnetoresistance (GMR) effect, describing the change of electrical resistivity in an external field [1,2].

It is of large interest to study the modification of the interlayer coupling and the GMR effect caused by a doping of the interfaces. Metallic Pd introduced between Fe and Cr should influence the coupling and the GMR-effect dramatically due to its large Pauli magnetic susceptibility.

The magnetic and magnetotransport properties of Fe/Cr/Pd/Fe multilayers deposited onto 5mm×10 mm GaAs(001) substrates have been investigated. The samples were prepared in a molecular beam epitaxy UHV system at a base pressure below 10^{-10} mbar. Masks have been used to produce up to four different samples with various thicknesses of Pd on a single substrate. The crystallographic structure of the films and their composition were monitored via *in situ* Auger Electron Spectroscopy (AES) and Low Energy Electron Diffraction (LEED).

The magnetization process of the Fe/Cr/Pd/Fe multilayers was investigated at room temperature by magneto-optical Kerr effect (MOKE) magnetometry. The MOKE curves for the two asymmetric multilayers GaAs/Fe (5 nm)/Cr (1 nm)/Fe (2nm)/Cr (2nm) and GaAs/Fe (5nm)/Cr (1 nm)/Pd (0.11 nm)/Fe (2 nm)/Cr (2 nm) are shown in Fig. 1. It is clearly seen, that the introduction of Pd dramatically changes the saturation field, which is proportional to the strength of the antiferromagnetic coupling.

The GMR-effect was studied in a temperature interval between 20 K and 300 K. A typical magnetoresistivity curve, measured at room temperature, is shown in Fig. 2. The value of the GMR-effect is defined as the difference between the measured values at zero field and at H=5 kOe, which exceeds the saturation fields of all investigated samples.

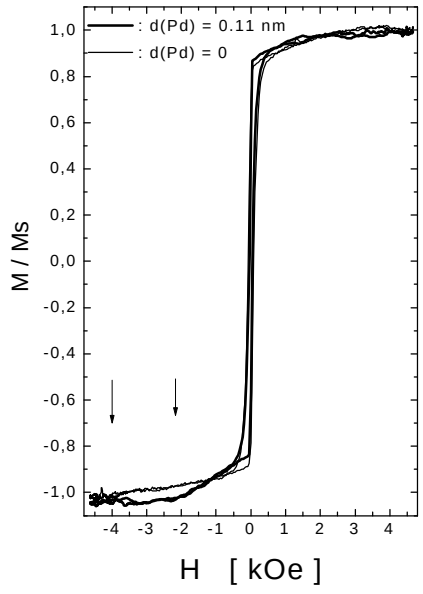

Fig. 1. Magnetization curves of GaAs/Fe (5 nm)/Cr (1 nm)/Pd/Fe (2 nm)/Cr (2 nm) multilayers for Pd-thicknesses, d_{Pd}=0 and 0.11 nm, measured at room temperature. The magnetic field is applied in-plane along the easy axis. The arrows indicate the saturation fields for both samples.

Fig. 1 and Fig. 2 demonstrate similar tendencies in the dependence of the strength of the anti-ferromagnetic coupling and the amplitude of the GMR-effect as a function of d_{Pd}.

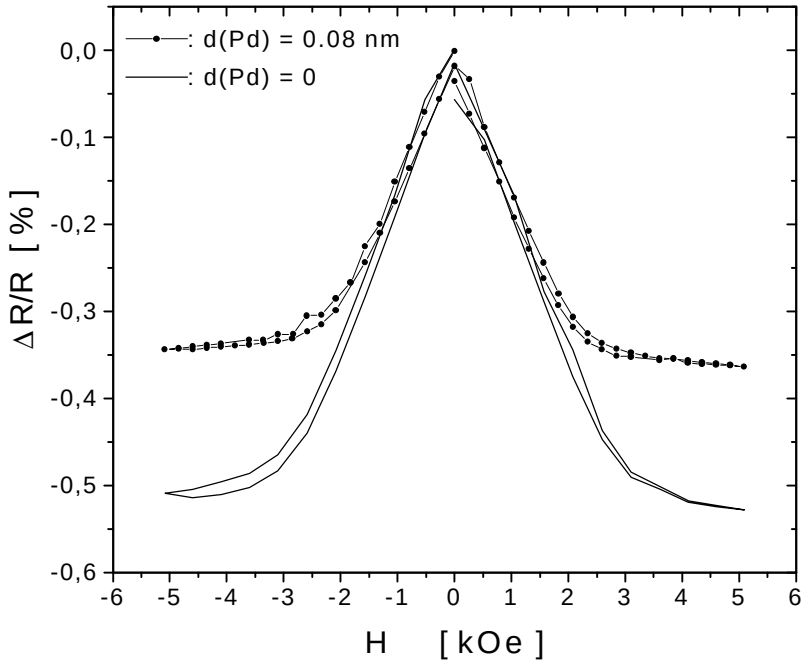

Fig. 2. Magnetoresistivity of GaAs/Fe (5 nm)/Cr (1 nm)/Pd/Fe (2 nm)/Cr (2 nm) multilayers for Pd-thicknesses, d_{Pd}=0 and 0.08 nm, measured at room temperature.

Both the strength of the coupling and the GMR amplitude decrease with increasing Pd thickness. However, the GMR-effect decreases with d_{Pd} faster than the saturation field, especially for small thicknesses of the Pd layer (see Fig. 3).

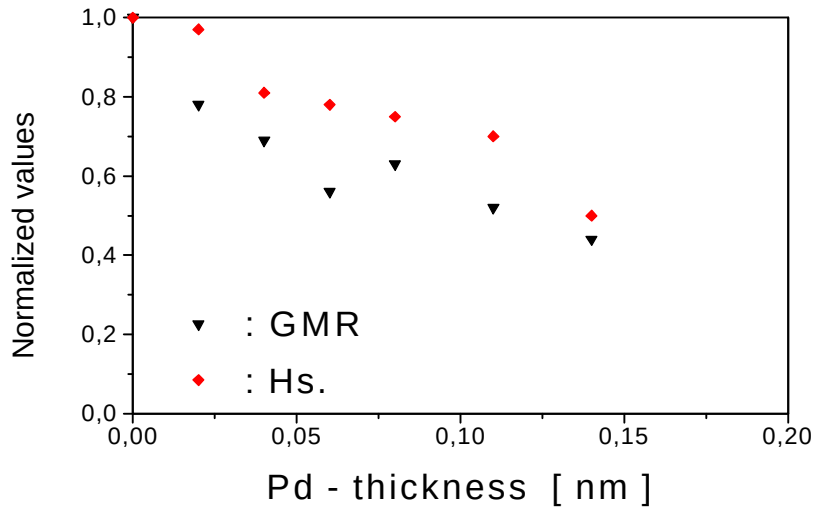

Fig. 3. GMR-effect and saturation field H_s in Fe/Cr/Pd/Fe multilayers as a function of the Pd - thickness, normalized to the corresponding values at d_{Pd}=0.

The observed difference indicates the fact that different mechanisms are responsible for the coupling and the GMR-effect in multilayers. Work is in progress to uncover the origin of these observations.

References

[1] P. Grünberg, R. Schreiber, Y. Pang, M. B. Brodsky, H. Sowers, Phys. Rev. Lett. 57, 2442 (1986).
[2] G. Binasch, P. Grünberg, F. Saurenbach, and W.Zinn, Phys. Rev. B 39, 482 (1989).

6.4 Brillouin light scattering investigations of exchange biased (110)-oriented NiFe/FeMn bilayers

C. Mathieu, M. Bauer, and B. Hillebrands[1]

The exchange bias effect, which results from exchange coupling between adjacent ferromagnetic (F) and antiferromagnetic (AF) layers, which are either deposited in a magnetic field or cooled down in a magnetic field after heating above the Néel temperature, is a well established phenomenon [1]. It manifests itself in a shift of the hysteresis loop along the axis of the applied field, the so-called exchange bias field, H_{eb}, and it is often described as an in-plane unidirectional anisotropy. Although exchange bias systems have been extensively studied [2-5], the microscopic origin of the exchange bias effect still remains unclear. The most advanced models propose the formation of magnetic domains in the AF layer causing a macroscopic exchange coupling strength of the experimentally observed size [6,7], which is two orders of magnitude smaller than the atomic F-AF exchange coupling strength. Key issues to be tested experimentally are, (i), to prove the assumption of large local, spatially variations of the F-AF coupling, and, (ii), apart from the detection of the unidirectional anisotropy, to search for possible additional anisotropy contributions of higher order induced by the exchange coupling mechanism.

We have chosen to study the (110)-oriented system of $Ni_{80}Fe_{20}/Fe_{50}Mn_{50}$ bilayers, since the lowest order in-plane anisotropy contributions, which are of unidirectional, of uniaxial and of fourfold symmetry, can be separately determined for simple symmetry reasons. An unexpected large uniaxial anisotropy contribution caused by the FeMn coverage has already been reported for this orientation. We have used Brillouin light scattering (BLS) from dipolar spin waves (Damon-Eshbach modes) propagating in the F-film parallel to the surface to extract the anisotropy constants [8].

Two MBE-grown staircase-shaped samples have been prepared on Cu(110) single crystal substrates. The samples consist of $Ni_{80}Fe_{20}$ films with thicknesses of 27 Å, 34 Å, 50 Å and 70 Å for the first, and of 18 Å, 24 Å, 37 Å and 90 Å for the second staircase-shaped sample. Half of each sample was covered by a 80 Å thick $Fe_{50}Mn_{50}$ layer. At this thickness the exchange bias effect is saturated. Finally, both samples were covered with a 20 Å and 30 Å thick protective Au layer, respectively. The samples were characterized using low energy electron diffraction, and their chemical cleanliness was checked by Auger electron spectroscopy. An analysis of the process parameters revealed that the residual oxygen content in the gas used for sputter cleaning was significantly larger during preparation of the second sample compared to the first. Evaporation on a slightly contaminated surface can therefore not be excluded for the second sample. During growth a magnetic field of ≈ 250 Oe was applied in the film plane along the $[1\bar{1}0]$ direction to induce exchange biasing. We note that the (110)-oriented $Fe_{50}Mn_{50}$ surface is an uncompensated plane with a resultant in-plane magnetization along the ±[001] directions.

The Brillouin light scattering experiments were performed with the external field applied in the film plane and in magnetic saturation to ensure a one-domain state of the F-film. Light of an Ar^+ ion laser with a wavelength of 514.5 nm and a power of 50 mW was focused onto the sample. The light inelastically scattered from thermally excited Damon-Eshbach modes was frequency analyzed using a fully automated tandem Fabry-Perot interferometer. From the spin wave dispersion curves measured

[1] in collaboration with J. Fassbender and G. Güntherodt, 2. Physikalisches Institut, RWTH Aachen, 52056 Aachen, Germany, R. Jungblut, J. Kohlhepp and A. Reinders, Philips Research Laboratories, Prof. Holstlaan 4, 5656 AA Eindhoven, The Netherlands

as a function of the in-plane angle, ϕ_H, of the external field, the free energy density, F_{ani}, was obtained. It is expressed as

$$F_{ani} = -K_s^{(2)} \cdot \cos^2 \theta + K_p^{(1)} \cos(\phi - \phi_{uni}) \cdot \sin\theta + K_p^{(2)} \cos^2 \phi \cdot \sin^2 \theta + K_p^{(4)} \cdot \cos^2 \phi \cdot \sin^2 \phi \cdot \sin^4 \theta . \quad (1)$$

with $K_s^{(2)}$ the perpendicular anisotropy constant, $K_p^{(1)}$, $K_p^{(2)}$ and $K_p^{(4)}$ the in-plane anisotropy constants of unidirectional, uniaxial and fourfold symmetry, respectively, and ϕ the in-plane angle of the direction of magnetization. ϕ_{uni} describes the reference direction of the unidirectional anisotropy. All in-plane angles are measured relative to the [001] direction. θ is the out-of-plane polar angle.

First we discuss the uncovered $Ni_{80}Fe_{20}$ staircase-shaped samples for reference. The measured spin wave frequencies as a function of ϕ_H are displayed in Fig. 1(a) for d_{NiFe} = 18 Å. For all layer thicknesses a nearly identical spin wave dependence on ϕ_H is obtained with a large uniaxial anisotropy contribution. The spin wave maxima which are present for the ±[001] directions indicate that the easy axis of magnetization is along [001]. The corresponding anisotropy field of about 600 Oe is much larger than the value of 5 Oe usually found in polycrystalline $Ni_{80}Fe_{20}$ films grown in an external field. Its origin is still unclear though it may well be of magneto-elastic origin and caused by the $Ni_{80}Fe_{20}$ growth mode of long (500 Å), narrow islands with a length-to-width ratio of approximately 10 lying along the magnetically hard [1$\bar{1}$0] direction, as has been shown by scanning tunneling microscopy.

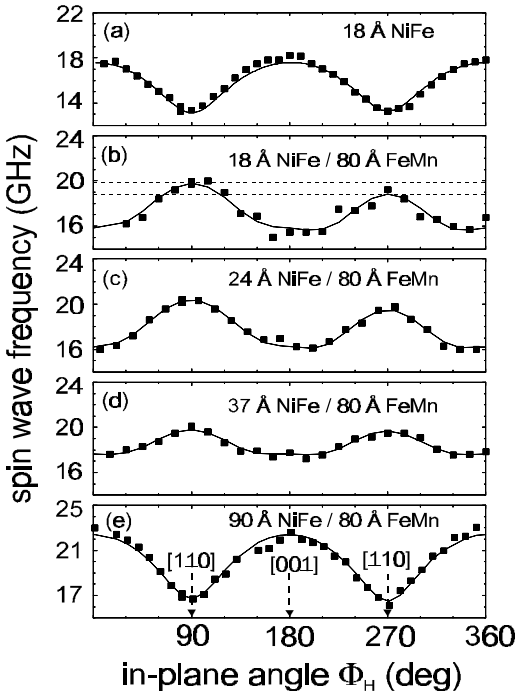

Fig. 1: Spin wave frequencies as a function of the angle of the in-plane applied field, ϕ_H, with the in-plane [001] direction for the Cu(110)/$Ni_{80}Fe_{20}$/(80 Å $Fe_{50}Mn_{50}$)/Au staircase-shaped sample with $Ni_{80}Fe_{20}$ layer thicknesses of 18 Å, 24 Å, 37 Å and 90 Å. The full lines are least squares fits. The difference in frequency of the spin wave maxima for the covered $Ni_{80}Fe_{20}$ layer of 18 Å thickness, representing the unidirectional anisotropy contribution, is indicated by the dashed horizontal lines. The applied field was 3 kOe.

Entirely different results are obtained upon covering the $Ni_{80}Fe_{20}$ layers by a 80 Å thick $Fe_{50}Mn_{50}$ layer as displayed in Fig. 1(b-e). For the $Ni_{80}Fe_{20}$ layer thicknesses of 18 Å to 37 Å, the spin wave maxima and thus the easy axes of magnetization are shifted by 90°. Moreover, for the 18 Å thick $Ni_{80}Fe_{20}$ layer, and to a lesser degree for the 24 Å and the 37 Å thick films, the two maxima at ϕ_H equal to 90° and 270° do not agree in their spin wave frequencies as indicated in Fig. 1(b) by the

dashed horizontal lines. The difference in frequency is a measure for the unidirectional anisotropy. From a model fit using Eq. (1) all anisotropy constants were determined. The results are displayed in Fig. 2 for the uncovered and covered $Ni_{80}Fe_{20}$ films, respectively. Again, first we discuss the uncovered samples (Fig. 2a,b,c). The in-plane fourfold anisotropy contribution is more or less zero. A large uniaxial in-plane anisotropy of $K_p^{(2)} = (-3\pm1)\cdot10^5$ erg/cm^3 is obtained nearly independent of the $Ni_{80}Fe_{20}$ thickness within the error margins. As expected the unidirectional anisotropy parameter, $K_p^{(1)}$, was found to be nearly zero within the error margins.

The anisotropy behavior of the covered $Ni_{80}Fe_{20}$ films is displayed in Fig. 2 (e,d,f). All three in-plane anisotropy contributions decrease with increasing $Ni_{80}Fe_{20}$ thickness. For large $Ni_{80}Fe_{20}$ thicknesses the respective anisotropy values of the uncovered and the covered $Ni_{80}Fe_{20}$ films converge indicating an interface effect. Within the given limited accuracy the differences in the respective anisotropy values are consistent with a $1/d_{NiFe}$ -scaling law for all three in-plane contributions. For the fourfold in-plane anisotropy, $K_p^{(4)}$, the data of the second sample agree only within a factor of two with those of the first sample. This is probably due to a lesser quality in the film-substrate interface due to problems in the sputter cleaning process (see above). However, both samples show the same systematic decrease of this anisotropy contribution with increasing $Ni_{80}Fe_{20}$ thickness. For the uniaxial in-plane anisotropy, $K_p^{(2)}$, a change in sign is obtained for the first sample at (35±5) Å and for the second sample near (50±10) Å. For the unidirectional anisotropy constant, $K_p^{(1)}$, we obtain for $Ni_{80}Fe_{20}$ film thicknesses smaller than about 40 Å (i.e. the range where reliable conclusions can be made) an angle for the reference direction of $\phi_{uni} = 90°$, i.e., the easy direction of the unidirectional and the easy axis of the uniaxial anisotropy contributions are collinear.

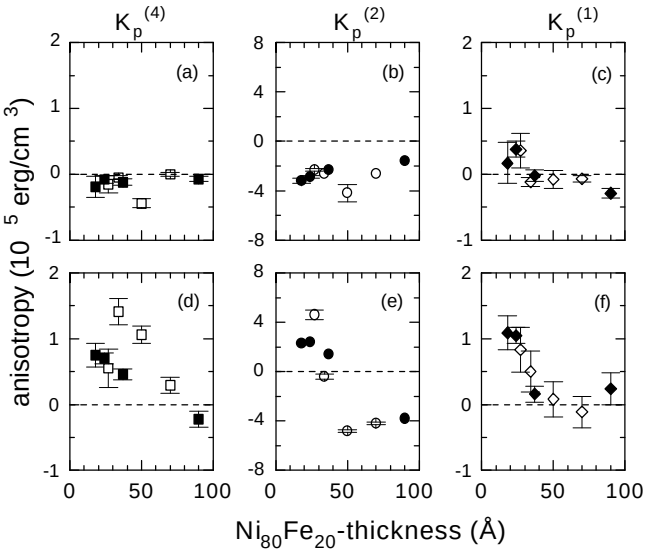

Fig. 2. Obtained anisotropy constants of the two staircase-shaped samples (open and closed symbols for the first and second sample) as a function of the $Ni_{80}Fe_{20}$ layer thickness for the uncovered layers (a,b,c) and the layers covered by 80 Å $Fe_{50}Mn_{50}$ (e,d,f).

While the origin of the unidirectional anisotropy contribution ($K_p^{(1)}$) is likely found in the exchange bias mechanism, the cause of the large modifications to the two other in-plane anisotropies ($K_p^{(2)}$, $K_p^{(4)}$), compared to the uncovered $Ni_{80}Fe_{20}$ films, needs to be discussed. Since these modifications are identified as interface contributions it is very likely that these contributions are also induced by the exchange coupling interaction and compete with the respective intrinsic contributions of the uncovered layer. Indeed, Jungblut et al. have recently shown that the exchange bias effect is causing the additional contribution in $K_p^{(2)}$.

We now turn to the measurements of the spin wave line widths. Mode broadening for propagating spin waves is obtained, if the internal fields vary locally on a length scale, which is of the order of the spin wave wavelength (3000 Å). In our experiments the spin wave modes show a large mode broadening of more than a factor of six upon covering the $Ni_{80}Fe_{20}$ layers by $Fe_{50}Mn_{50}$ for the lower $Ni_{80}Fe_{20}$ layer thicknesses. This is displayed in Fig. 3 for the 24 Å thick $Ni_{80}Fe_{20}$ layer for the covered and uncovered case. For the covered sample the mode width varies within a factor of two as a function of the azimuthal angle, ϕ_H. As can be seen from Figs. 1 and 3 the maximum and minimum values correspond to the hard [001] and easy $[1\bar{1}0]$ direction of magnetization, respectively. The line width is strongly decreasing with increasing $Ni_{80}Fe_{20}$ layer thickness converging to the width of the uncovered $Ni_{80}Fe_{20}$ films. This is also characteristic for an interface effect.

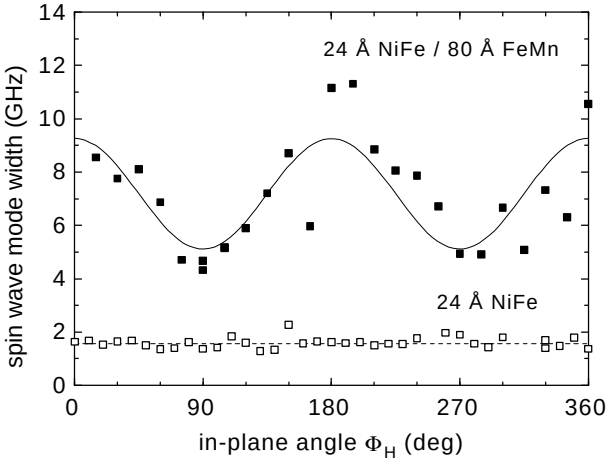

Fig. 3. Spin wave mode widths as a function of the angle of the in-plane applied field, ϕ_H, with the in-plane [001] direction for the 24 Å thick $Ni_{80}Fe_{20}$ layer for the $Fe_{50}Mn_{50}$ covered and uncovered case. The full (open) squares are the data of the covered (uncovered) layer. The full and dashed lines are guides to the eye.

The large spin wave mode broadening and its dependence on the in-plane angle of the external field can be understood as follows: We assume variations in the local F-AF exchange field on a scale of the atomic terrace width, which is of the order of 50 Å [6]. From the local exchange field the macroscopic, averaged exchange bias field, or equivalently, the unidirectional in-plane anisotropy, are generated. The variations in the F-AF exchange field will cause a broadening of the spin wave line width, which is therefore a characteristic fingerprint of the variations [8-10]. The broadening is largest, if not only internal field contributions (here the exchange coupling field) vary, but also the direction of magnetization. The latter occurs, if the easy axis of the spatially varying internal field is not collinear with the external field. By changing the direction of the external field minima and maxima in the line width appear at the easy and hard axes of the dominating, exchange coupling induced uniaxial anisotropy.

In conclusion, for the (110)-oriented $Ni_{80}Fe_{20}/Fe_{50}Mn_{50}$ exchange bias system large in-plane anisotropy contributions of unidirectional, uniaxial and fourfold symmetry have been found. In particular we observed an in-plane switching of the easy axis of magnetization with increasing $Ni_{80}Fe_{20}$ layer thickness from the $[1\bar{1}0]$-axis to the [001]-axis. The observed large spin wave mode width in the bilayer structures is a clear indication for large local variations of the exchange coupling. The decreasing of the mode width with increasing $Ni_{80}Fe_{20}$ layer thickness is consistent with the nature of an interface effect.

References

[1] W.H. Meiklejohn and C.P. Bean, Phys. Rev. **102**, 1413 (1956); Phys. Rev. **105**, 904 (1957).
[2] W. Stoecklein, S.S.P. Parkin, and J.C. Scott, Phys. Rev. B **38**, 6847 (1988).
[3] M.J. Carey, A.E. Berkowitz, J. Appl. Phys. **73**, 6892 (1993).
[4] R. Jungblut, R. Coehoorn, M.T. Johnson, J. aan de Stegge, A. Reinders, J. Appl. Phys. **75**, 6659 (1994).

[5] R. Jungblut, R. Coehoorn, M.T. Johnson, Ch. Sauer, P.J. van der Zaag, A.R. Ball, Th. G.S.M. Rijks, J. aan de Stegge, A. Reinders, J. Magn. Magn. Mater. **148**, 300 (1995).
[6] R. Jungblut, M.J. Decker, J.T. Kohlhepp, J.J. de Vries, K. Ramstöck, A. Reinders, R. Coehoorn, to be published.
[7] N.C. Koon, to be published.
[8] B. Hillebrands, Phys. Rev. B **44**, 12417 (1991).
[9] R.L. Stamps, R.E. Camley, B. Hillebrands, G. Güntherodt, Phys. Rev. B **47**, 5072 (1993).
[10] B. Hillebrands, J.V. Harzer, G. Güntherodt, J.R. Dutcher, J. Magn. Soc. Jpn. **17**, 17 (1993).

6.5 Angular dependence of the exchange bias field in the NiFe/FeMn (110) exchange bias system

S. Riedling, M. Bauer, C. Mathieu, and B. Hillebrands[1]

The phenomenon of exchange biasing was first observed in 1957 by Meiklejohn and Bean in the Co/CoO System [1]. They found that systems consisting of a ferromagnetic and an antiferromagnetic material show a shifted hysteresis curve if grown in a magnetic field or heated above the Néel-temperature while a magnetic field is applied. In general, exchange biasing is considered to be the result of the exchange interaction between the ferromagnetic and the antiferromagnetic layer at the interface. Although there was a lot of progress in the modelling of such systems, the mechanism responsible for exchange biasing as well as the correlation with the interfacial spin structure is still a subject of discussion. Recently Jungblut et al. published measurements of the exchange bias effect in FeNi/FeMn bilayer wedges on Cu substrates with the three principal orientations [2]. They found that the exchange bias field H_{eb} as well as the coercivity field H_c depend on the crystal orientation and therefore on the interface structure, but no indication for a preference of an uncompensated (110)-orientation or a compensated (100)- and (111)-orientaton was observed. They also observed a large uniaxial anisotropy contribution caused by the FeMn coverage in the (110) oriented $Ni_{80}Fe_{20}/Fe_{50}Mn_{50}$ bilayer system. The uniaxial symmetry direction depends on the thickness of the NiFe layers and turns from $[1\bar{1}0]$ to [001] near 60Å with increasing thickness.

In order to investigate the interplay between the exchange bias effect and modifications of the magnetic anisotropies we chose to investigate the (110)-oriented $Ni_{80}Fe_{20}/Fe_{50}Mn_{50}$ bilayer system grown onto single crystal Cu(110) substrates at the Phillips Research Laboratories. Four independent anisotropy contributions exist, which are, within the film plane, the unidirectional anisotropy, the uniaxial anisotropy, the cubic anisotropy, and, perpendicular to the film plane, the perpendicular anisotropy. The study was performed by preparing bilayers with varying $Ni_{80}Fe_{20}$ thickness and by analyzing the magnetization reversal process. The in-plane angular-dependent measurement of H_{eb} allows to quantitatively determine all contributing in-plane anisotropies by fitting the experimental data. For the simulations the following expression for the free energy is assumed:

$$\begin{aligned} F_{ani} = &+K_p^{(1)} \cos(\phi - \phi_{uni}) && \textit{unidirectional anisotropy contribution} \\ &+K_p^{(2)} \cos^2(\phi) && \textit{uniaxial anisotropy contribution} \\ &+K_p^{(4)} \cdot \cos^2(\phi) \cdot \sin^2(\phi). && \textit{fourfold anisotropy contribution} \end{aligned} \quad (1)$$

with ϕ, the angle between the direction of magnetization and the [001]-direction. ϕ_{uni} describes the reference direction of the unidirectional anisotropy with respect to the $[1\bar{1}0]$-direction.

The samples were grown by MBE onto a Cu (110) single crystal substrate. By moving an eclipsing shutter bilayers with four different permalloy ($Ni_{80}Fe_{20}$) layer thicknesses of 18 Å, 24 Å, 37 Å and 90 Å were prepared. Half of the layers are covered with a 80Å $Fe_{50}Mn_{50}$ film, which is thick enough to saturate the exchange bias effect. During the growth of the sample a field of 250 Oe along the $[1\bar{1}0]$ direction was applied in the film plane. All hysteresis loops were measured at room temperature using the longitudinal magneto-optical Kerr effect (MOKE).

[1] in collaboration with R. Jungblut, J. Kohlhepp and A. Reinders, Philips Research Laboratories, Prof. Hostlaan 4, 5656 AA Eindhoven, The Netherlands.

First we will discuss the results of the uncovered $Ni_{80}Fe_{20}$ reference layers. We observe no exchange bias field but a strong uniaxial anisotropy for all thicknesses with the easy axis of magnetization uniformly pointing along the [001] direction. From the measured saturation fields, $K_p^{(2)}$ was obtained. Its value of $(-3.5\pm0.3)\times10^5$ erg/cm^3 is independent of the thickness. STM images show that the $Ni_{80}Fe_{20}$ films grow as long narrow islands along the $[1\bar{1}0]$ direction which has been identified as the magnetically hard direction [3]. This indicates that the observed uniaxial anisotropy is likely to be of magnetoelastic origin.

In contrast, $Ni_{80}Fe_{20}/Fe_{50}Mn_{50}$ bilayers show a strong exchange bias effect as well as a strong uniaxial anisotropy with the easy axis switching from $[1\bar{1}0]$ to [001] near 40 Å as discussed above. In Fig. 1a-d, the measured exchange bias fields are plotted as a function of the in-plane angle of the applied field for all four $Ni_{80}Fe_{20}$-layer thicknesses. The full lines represent a fit using Eq. (1).

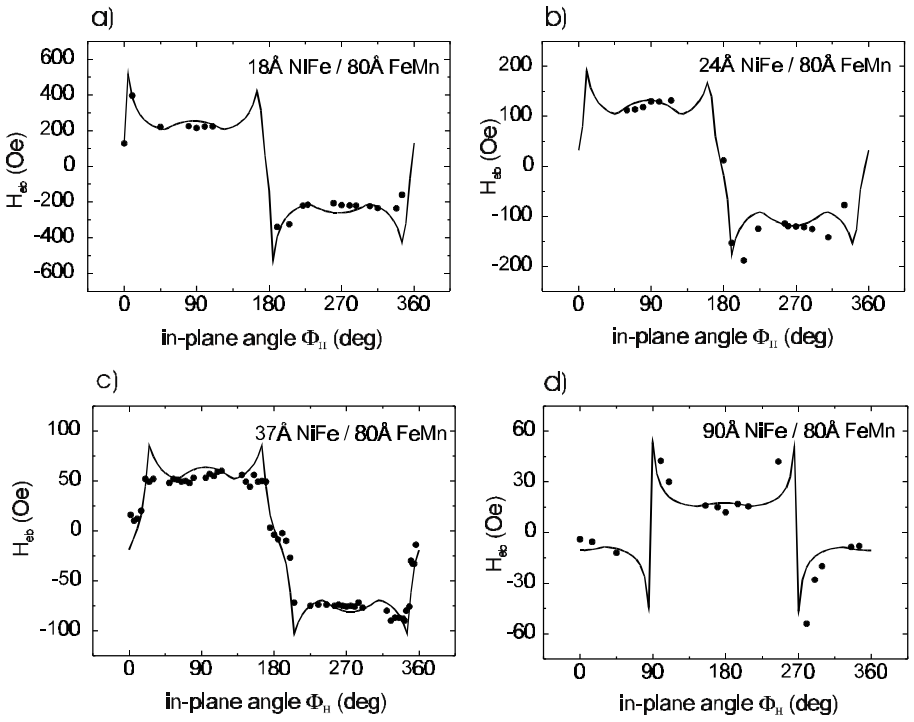

Fig. 1. in-plane angular dependence of the measured exchange bias field for NiFe thicknesses of a) 18 Å, b) 24 Å, c) 37 Å and d) 90 Å.

The exchange bias effect is is clearly observed for all investigated $Ni_{80}Fe_{20}$ thicknesses. For d_{NiFe} = 90 Å a shift of 90° is observed in the data, indicating that the symmetry direction rotates from $[1\bar{1}0]$ for smaller $Ni_{80}Fe_{20}$ thicknesses to [001].

The exchange bias field varies by no means like a sin or cos function. This is indicative for the strong interplay between the unidirectional, the uniaxial and the cubic anisotropy contributions for the easy direction of magnetization. In the vicinity of the hard axis of the in-plane uniaxial anisotropy, where the exchange bias field changes sign, an enhancement of the exchange bias field of up to a factor of two is observed. The fit represents the experimental data very well indicating that the remagnetization process is purely a rotation of the magnetization. Due to the high sensitivity of the exchange bias field to all in-plane anisotropy contributions, very precise values of the corresponding anisotropy constants and the directions of the respective symmetry axes are obtained from the fitting procedure.

In Fig. 2 the obtained unidirectional anisotropy constants $K_p^{(1)}$ and $K_p^{(2)}$ are plotted as a function of the $Ni_{80}Fe_{20}$ thickness in comparison with data determined by Brillouin light scattering (BLS) [4]. In the case of the uniaxial anisotropy, a pronounced thickness dependent contribution favoring the

[$1\bar{1}0$]direction, induced by the FeMn layer, is observed. This contribution, in competition with the thickness independent twofold anisotropy of the uncovered permalloy layer, causes a switching of the uniaxial easy axis as evidenced by the change of sign in $K_p^{(2)}$. From a $1/d_{NiFe}$ fit, the critical thickness for the switching of the uniaxial anisotropy from [001] to [$1\bar{1}0$] is estimated to be 40 Å. The easy axis of the interlayer-exchange induced uniaxial contribution is perpendicular to the directions of the layer magnetizations in the antiferromagnetic layer. Therefore the two opposite domain directions in the antiferromagnetic layer could lead to a frustration effect and force the interfacial magnetization of the $Ni_{80}Fe_{20}$ layers to turn perpendicular to its initial direction. This origin is analogous to the origin of the biquadratic coupling effect between two magnetic layers [5].

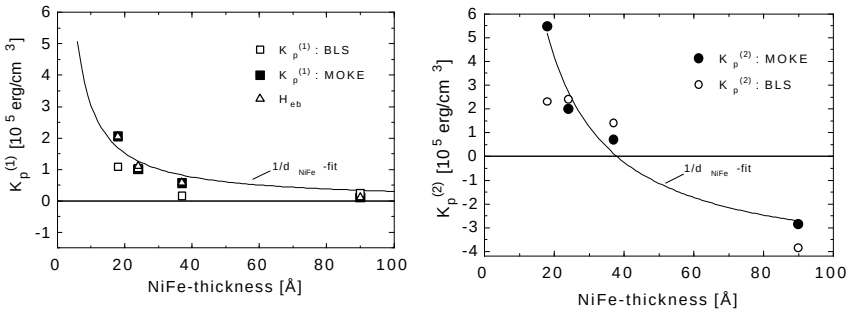

Fig. 2. Obtained unidirectional (left) and uniaxial (right) anisotropy constants as a function of the $Ni_{80}Fe_{20}$ layer thickness compared with data obtained from Brillouin light scattering measurements. The solid lines are $1/d_{NiFe}$-fits. Note the switching of both symmetry axes equivalent to the change of sign of $K_p^{(2)}$ at a $Ni_{80}Fe_{20}$ thickness of about 40 Å.

With these informations about the twofold anisotropy data of the layers, the anomalous unidirectional anisotropy axis of the 90 Å $Ni_{80}Fe_{20}$/80Å $Fe_{50}Mn_{50}$ layer, which is pointing perpendicular to the direction of the growth field, can be understood. For permalloy an uniaxial anisotropy constant of about 3.5×10^5 erg/cm^3 corresponds to a saturation field H_s of 1 kOe along the magnetically hard direction. Thus the applied growth field of 250 Oe is not strong enough to saturate the magnetization of the pure $Ni_{80}Fe_{20}$ layers, as well as the one of the 90 Å $Ni_{80}Fe_{20}$ /80 Å $Fe_{50}Mn_{50}$ layer, along the [$1\bar{1}0$] direction. The easy direction of the unidirectional anisotropy is determined by the direction of magnetization during the deposition of the FeMn layer.

The spin structure of γ-FeMn is compensated along the [$1\bar{1}0$] direction but uncompensated along the [001] direction. We observed the exchange bias effect in both directions, only dependent on the direction of the magnetization in the ferromagnetic layer during growth. Thus, in accordance with the results of Jungblut et al., the ideal, interfacial spin orientation seems to play no fundamental role. It is most likely that roughness causes partially uncompensated interfaces in both directions.

References

[1] W.H. Meiklejohn, C.P. Bean, Phys. Rev. Lett. **102**, 1413 (1956); Phys. Rev. Lett. **105**, 904 (1957).
[2] R. Jungblut, R. Coehoorn, M.T. Johnson, J. aan de Stegge, A. Reinders, J. Appl. Phys. **75**, 6659 (1994); R. Jungblut, R. Coehoorn, M.T. Johnson, Ch. Sauer, P.J. van der Zaag, A.R. Ball, Th. G.S.M. Rijks, J. van de Stegge, A. Reinders, J. Magn. Magn. Mater. **148**, 300 (1995).
[3] R. Jungblut, M.J. Decker, J.T. Kohlhepp, J.J. de Vries, K. Ramstöck, A. Reinders, R. Coehoorn, to be published.
[4] C. Mathieu, M. Bauer, B. Hillebrands, J. Fassbender, G. Güntherodt, R. Jungblut, J. Kohlhepp, A. Reinders, J. Appl. Phys., in press.
[5] J. C. Slonczewski, Phys. Rev. Lett. **67**, 3172 (1991); B. Dieny, A Vedyayev, Europhys. Lett. **25**, 723 (1994).

6.6 Magnetic properties of atomically layered Fe/Au multilayers

N. Knorr, U. Schuth, S. Riedling, J. Jorzick, C. Mathieu, S.O. Demokritov, and B. Hillebrands[1]

Atomically layered Fe(001)/Au(001) multilayers provide an excellent testing ground for investigations of the development of the magnetic order and of anisotropies upon the transition from a two-dimensional to a three-dimensional atomic arrangement due to the immiscibility and the excellent growth properties of the two constituent materials. We have studied multilayers with the thickness of the Fe layers of 1 and 2 monolayers (ML) and the thickness of the Au layers in the range between 1 and 6 ML, the number of monolayers always being an integer value. The number of bilayers is 30. The multilayers were grown at the IFF, FZ Jülich using e-beam evaporation in a MBE system. The substrates are cleaved MgO(001) single crystals. The samples are listed in Table 1.

Sample	**Composition**	**direction of M_s**	**T_c [K]**	**$4\pi M_{s@300\,K}$ [G]**	**H_c at 10 K [Oe]**	**a_R**
A	[Fe 1/Au 1]	in plane	>500	5940	266	0,98
B	[Fe 1/Au 1]	in plane	>500	7595	227	0,67
C	[Fe 1/Au 2]	out of plane	463	3953	193	0,59
D	[Fe 1/Au 2] on GaAs	out of plane	>500		194	
E	[Fe 1/Au 3]	out of plane	334	1365	629	0,21
F	[Fe 1/Au 3]	out of plane	344	1795	810	0,39
G	[Fe 1/Au 4]	out of plane	325	659	1003	
H	[Fe 1/Au 5]	out of plane	300	0	1385	
I	[Fe 1/Au 6]	out of plane	210	0	3440	
J	[Fe 2/Au 1]	in plane	>500	10932	130	
K	[Fe 2/Au 3]	out of plane	>500	7862	24	
L	[Fe 2/Au 4]	out of plane	>500	6595	40	

Table 1: Prepared samples. The numbers in the second column indicate the numbers of monolayers for each Fe and Au layer. Listed are the direction of the spontaneous magnetization, the Curie temperature T_C , the room temperature saturation magnetization $4\pi M_s$, the 10 K coercivity field H_c, and the ratio a_R of the temperature, at which the remanent magnetization starts to deviate from M_s, to T_c.

The magnetic properties of the multilayers are studied by Brillouin light scattering (BLS), vibrating sample magnetometry (VSM), polar and longitudinal Kerr magnetometry and by SQUID magnetometry (FZ Jülich) in the temperature range of 2 K-400 K.

In Tab. 1 the obtained room temperature saturation magnetization M_s, the Curie temperature T_C, the 10 K coercivity field H_c, and the ratio a_R of the temperature, at which the remanent magnetization starts to deviate from M_s, to T_C are listed. With increasing gold layer thickness the coupling between the magnetic layers, which is dipole-dipole coupling and/or RKKY interaction [1], decreases. This is evidenced by the decrease of T_C with increasing gold layer thickness as well as by the decrease of M_s (only a negligible magnetic moment is induced in the Au atoms [2]).

[1] in collaboration with R. Schreiber and P. Grünberg, IFF, Forschungszentrum Jülich, Germany.

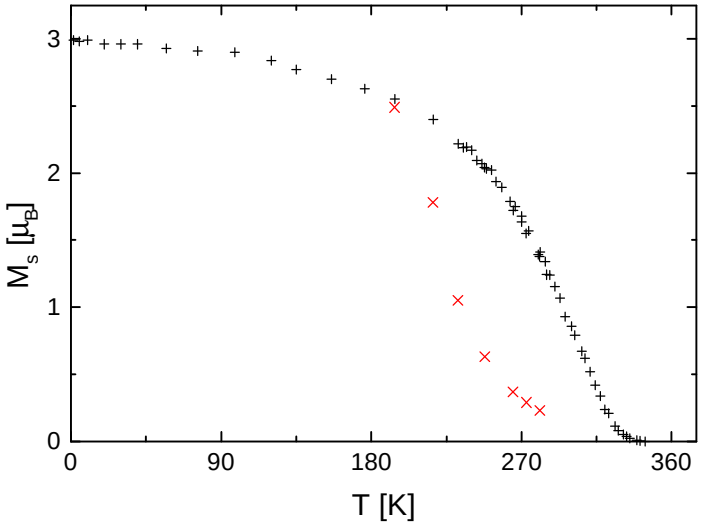

Fig. 1. Temperature dependence of the saturation magnetization (upper curve) and the remanence (lower curve) of the [Fe 1/Au 4] sample, obtained by polar Kerr magnetometry. The measurements are calibrated to the T=0 K value of 2.76 μB [3].

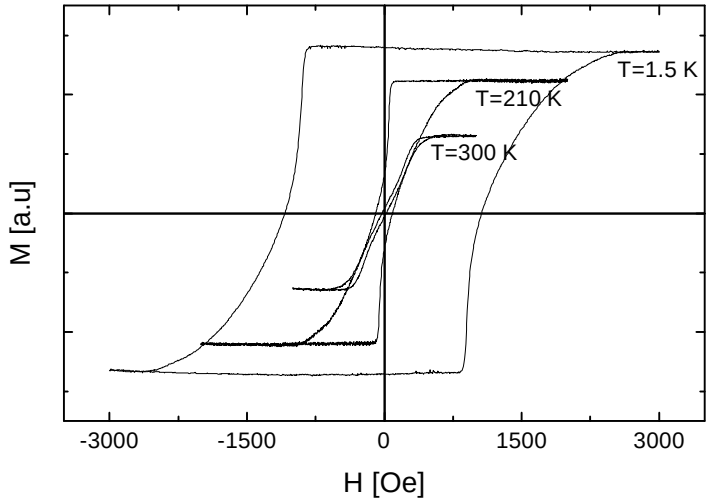

Fig. 2. Magnetization curves of the [Fe 1/Au 3] sample measured by polar MOKE magnetometrie. Please note that the curves (especially at 300 K) are concavely shaped.

The samples C to I with only one Fe ML and spontaneous out-of-plane magnetization (see Tab. 1) exhibit striking changes in the shape of their magnetization curves with temperature (Fig. 2). At high temperatures, the curves can be described by a model [4], which assumes infinitely thin and freely mobile domain walls. The magnetization at different magnetic fields is calculated by minimizing three competitive energies - the demagnetizing- , the wall- , and the field energy. This model yields a concave shape of the curves and no coercivity; it can be applied on [Fe 2/Au 3] and [Fe 2/Au 4] over the entire measured temperature region. At low temperatures, the curves are of square shape, and the coercivity field increases strongly (Fig. 3), which is probably due to aftereffects. The effects are more pronounced for thicker gold layers (see the last two columns of Tab. 1). For temperatures in between, the slope of the curves in combination with the aftereffect leads to a rapid decay of the remanent magnetization (Fig. 1).

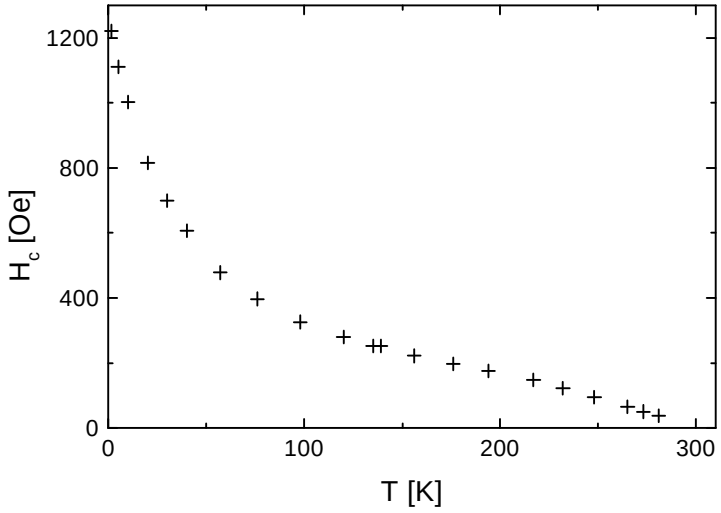

Fig. 3. Temperature dependence of the coercivity field of the [Fe 1/Au 4] sample.

The perpendicular anisotropy constant $K_s^{(2)}$ can be derived from the dependence of the spin wave frequencies on the applied field. Using the free energy expression

$$F = K_s^{(2)} \cos^2(\vartheta) + 2\pi Ms^2 \cos^2(\vartheta) + ... \quad (1)$$

with ϑ the angle between the direction of the magnetization and the direction normal to the multilayer plane, we observe that $K_s^{(2)}$ varies like M_s^2 as a function of temperature (Fig. 4).

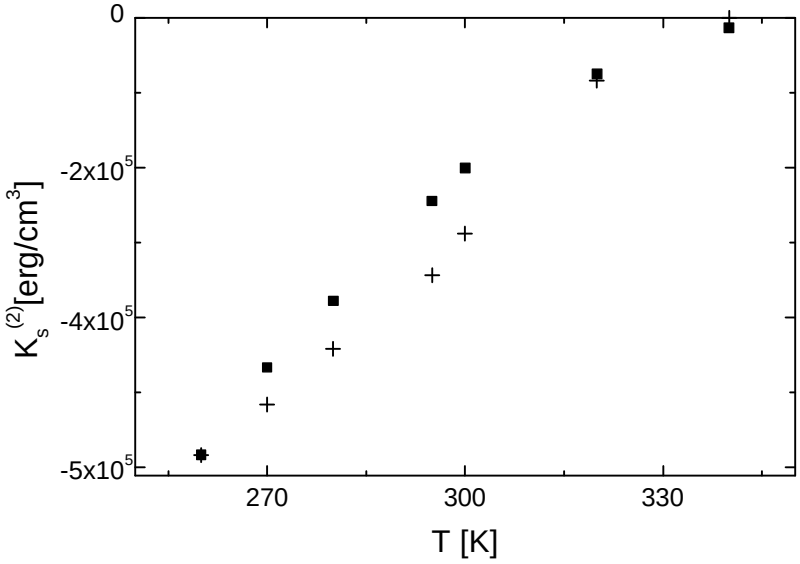

Fig. 4. Temperature dependence of $K_s^{(2)}$ of the [Fe 1/Au 3] sample. M_s^2, calibrated to the 260 K value of $K_s^{(2)}$, is marked by crosses.

References

[1] H. Yamazaki, Phys. Stat. Solidi B **197**, 195 (1996).
[2] Z. Shi, J.F. Cooke, Z. Zhang, Phys. Rev. B **54**, 3030 (1996).
[3] J.M. MacLaren, M.E. McHenry, S. Crampin, M.E. Eberhart, J. Appl. Phys. **67**, 5406 (1990).
[4] H.J.G. Draaisma, W.J.M. de Jonge, J. Appl. Phys. **62,** 3318 (1987).

6.7 Laser Interference Lithography

P. Kimmel, M. Bauer, and B. Hillebrands

For magnetic storage media and sensors to be developed in the forthcoming years it is becoming essential to gain knowledge about the magnetic properties of films patterned in the sub-µm range. One key problem is to develop patterning procedures which allow for a fast process over a large sample area. We have installed a laser interference lithography (LIL) machine, which is specified to pattern magnetic films of up to 1 cm^2 with periodic structures down to a periodicity of 176 nm. The system allows for fast and precise patterning process and it is complementary to standard electron beam (EBL) or X-ray lithography techniques.

This year we have set up a clean-room facility containing the LIL machine and a class-100 laminar flow box for the photoresist processing. The LIL setup is illustrated schematically in Fig. 1. A light beam of an Ar-ion laser (wavelengths used: 351 and 458 nm) is expanded and filtered by a spatial filter comprising a focus lens and a pinhole. After the pinhole the divergent beam of high wavefront quality reaches in one part directly the resist-coated sample and in the other part a mirror which redirects this part of the beam onto the sample. Both beams generate a periodic stripe interference pattern in the photoresist. The method is much faster than EBL, in particular if large areas need to be structured. The pattern period can be chosen down to half of the used wavelength, i.e. 176 nm.

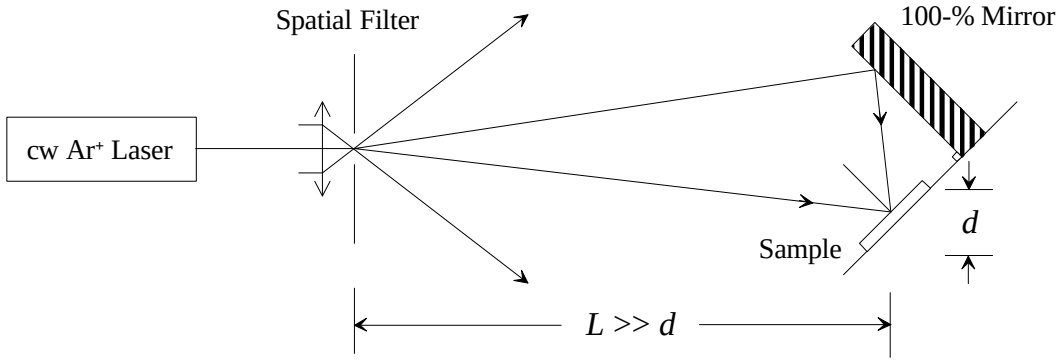

Fig. 1. Schematic view of the laser interference lithography setup

We are using standard resists which are diluted to achieve a resist layer thickness below 100 nm. All process parameters like exposure dose, developing time or baking temperatures have been optimized in order to achieve an optimum quality of the patterned structures.

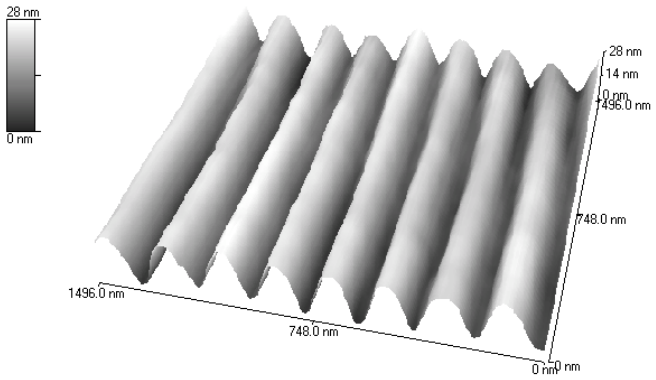

Fig. 2. AFM micrograph of the smallest produced wires in the photoresist.

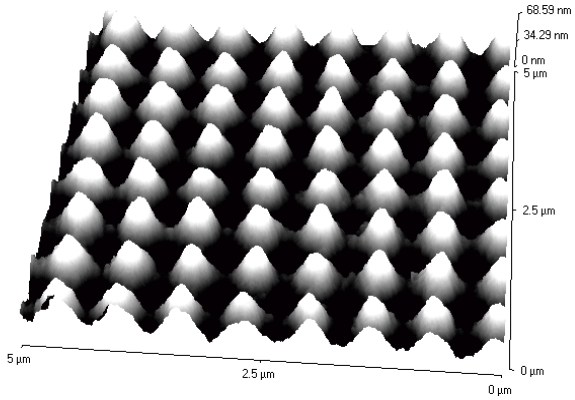

Fig. 3. AFM micrograph of a dot array, which is generated by two exposures with a 90° rotation of the sample in between.

Currently we optimize the transfer process of the photoresist patterns into the magnetic films using a plasma beam source with Ar^+ ions and ion beam etching (IBE).

As a first test structure the stripe patterns in the resist have been transferred into the silicon surface generating a periodic corrugation of 187 nm with an amplitude of 3 nm. Brillouin light scattering experiments have been performed to search for anomalies in the dispersion of the Rayleigh phonon mode. Anomalies are reported, which appear if the wavelength of the Rayleigh mode equals the corrugation periodicity (zone folding effect) [1]. Fig. 4 shows a typical Brillouin light scattering spectrum, demonstrating the splitting of the Rayleigh mode.

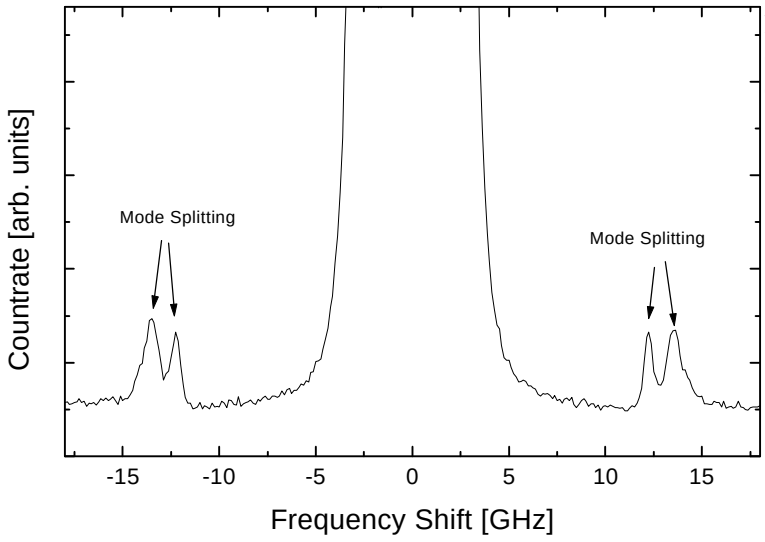

Fig. 4. Splitting of the surface phonon (Rayleigh mode) on corrugated silicon, observed by Brillouin light scattering.

As a second test case we studied the magnetic anisotropy induced by the shape effect in an array of magnetic $Ni_{80}Fe_{20}$ wires. A 150 Å thick $Ni_{80}Fe_{20}$ film was grown onto Si/SiO_2 substrates using an e^--beam evaporator. The exposed photoresist structure was transferred into the $Ni_{80}Fe_{20}$ film using IBE after optimization of the etching process parameters (ion energies, ion current, rf power). Samples with a periodicity of 700 nm and a $Ni_{80}Fe_{20}$ stripe width of 230 nm have been produced. Fig. 5 shows an AFM micrograph of the obtained structures. The uniformity of the obtained $Ni_{80}Fe_{20}$ wires is satisfactory over a large sample area.

The magnetization curves have been measured using the longitudinal magneto-optical Kerr effect with the field aligned parallel and perpendicular to the wires. The data is displayed in Fig. 5. A large anisotropy between both field geometries is clearly visible. The coercive field is considerably larger

compared to the data obtained from the unpatterned regions of the sample indicating that the number

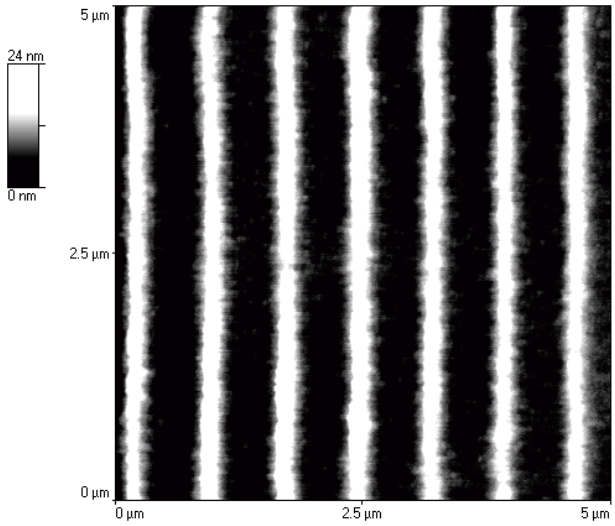

Fig 4. AFM micrograph of the wires etched in permalloy.

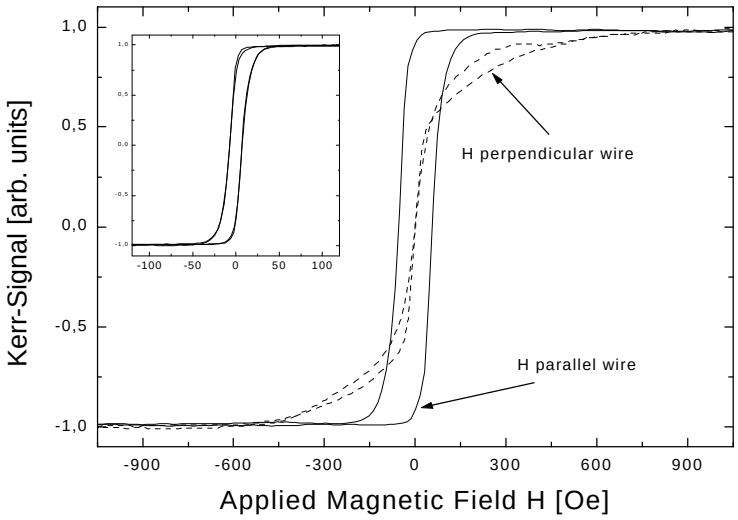

Fig. 5. Magnetisation reversal behaviour of the magnetic wires displayed in Fig. 4. The inset shows the hysteresis curve of the non-patterned film.

of pinning centers is increased by the patterning process.

References

[1] J.R. Dutcher, B. Hillebrands, S. Lee, G.J. McLaughlin, G.I. Stegeman, Phys. Rev. Lett. **68**, 2464 (1992).

6.8 Static and dynamic properties of patterned magnetic permalloy films

B. Hillebrands, C. Mathieu, C. Hartmann, M. Bauer, O. Büttner, S. Riedling, B. Roos, and S.O. Demokritov[1]

The physical properties of magnetic particles on the micro- and nanometer scale have attracted much interest in the last few years especially because of the promising prospects in future data storage and sensor applications [1-6]. There remain many unresolved problems in the preparation and characterization of these structures, and therefore suitable preparation procedures and analysis tools are still under development. It is of particular importance to develop fabrication methods for magnetic islands with a very narrow distribution of the magnetic parameters and with well controlled coupling between the islands, which for many applications should be made negligibly small. In particular a precise control of magnetic anisotropies induced by the patterning process as well as by finite size effects is required. Here we report on studies of regular square arrays of magnetic dots by Brillouin light scattering (BLS), Kerr magnetometry and magnetic force microscopy. From the measured spin wave dispersion properties obtained from the BLS experiments the uniformity of the magnetization distribution, demagnetizing effects as well as coupling strengths between magnetic dots are obtained.

Well separated dots of circular shape made of polycrystalline permalloy ($Ni_{80}Fe_{20}$) will not exhibit any in-plane anisotropy. For dots with small enough separation any observed in-plane anisotropy is therefore a fingerprint for anisotropic, magnetic coupling between the dots. Measurements of coupling induced anisotropies allow for a quantitative study of magnetic interdot coupling.

The method of choice is Brillouin light scattering from dipolar dominated spin wave modes (Damon-Eshbach modes) propagating within the dots [7]. The spin wave frequencies depend on the demagnetization factor of each dot, on the value and distribution of the magnetization vector, on anisotropies, and to a weak degree on the volume exchange constant. A study of the mode dispersion and of the dependence on the in-plane direction of the external field allows to determine the interdot coupling strength.

We have studied regular square lattices of circular shaped dots of permalloy of 1 μm and 2 μm diameter and 500 Å and 1000 Å thickness. The films were prepared in ultrahigh vacuum onto Si/SiO_2 10x10 mm^2 substrates using an e^--beam evaporator. The samples were patterned by synchrotron radiation based X-ray lithography performed at the L2M synchrotron station at the super ACO storage at LURE, Orsay, using ion beam etching to transfer the patterns into the permalloy films. A subtractive process was used as described elsewhere [8]. Each sample consists of circular dots arranged in a 1x1 mm^2 square lattice with a diameter/periodicity of 1/1.1, 1/2, 2/2.2 and 2/4 μm, respectively. For comparison, and in order to check for modifications of the magnetic bulk properties during the patterning process, the remaining parts of the samples were not patterned, i.e. consist of a continuous film. Depth profile measurements show that the etching process cuts 200 Å deep into the substrate between the dots, which guarantees that $Ni_{80}Fe_{20}$ bridges between the dots do not exist. Electron micrographs show as well that neighboring dots are not touching.

The Brillouin light scattering experiments were performed in backscattering geometry using a digitally controlled, fully automated multipass tandem Fabry-Perot interferometer with the in-plane mo-

[1] in collaboration with B. Bartenlian, and C. Chappert, IEF, Université Paris Sud, 91405 Orsay, France, D. Decanini, F. Rousseaux, and E. Cambril, L2M, Bagneux, France A. Müller, B. Hoffmann, and U. Hartmann, Universität Saarbrücken, Germany

mentum transfer perpendicular to the applied magnetic field. Ar^+-ion laser light with an incident power of at most 100 mW and an angle of incidence of 45° degrees was focused onto the sample with a focus diameter of about 40 µm. The spin wave frequencies were detected as a function of the strength, H, and the angle, Φ_H, of the in-plane applied magnetic field.

The magnetization reversal behavior as well as the zero field domain structure have been investigated using Kerr magnetometry and magnetic force microscopy. Kerr loops have been measured as a function of the angle Φ_H of the in-plane applied field. The focus diameter of the probing laser light was below 0.3 mm to ensure alignment within the patterned area. Magnetic force microscope images have been made at zero applied field using a Co coated Si-cantilever at a sample distance between 10 and 100 nm at a vibration frequency of 69.62 kHz. The spatial resolution is below 100 nm.

A detailed BLS study of the dependence of the spin wave properties on the applied magnetic field has been performed. Fig. 1 shows a typical Brillouin light scattering spectrum. The scattering geometry is shown in the inset of Fig. 2. At zero frequency the elastically scattered light, and at frequencies of ±(33–37) GHz the ghost peaks are observed. In the regions of ±(6.5–22) GHz the inelastically scattered signal is recorded. We observe the Damon-Eshbach mode, the first standing spin wave (volume mode) and a surface phonon (see Fig. 1). The obtained spin wave dispersion is shown in Fig. 2 for the 2/2.2 µm sample.

With negligibly small anisotropies [9], as obtained for the permalloy film, the frequency of the Damon-Eshbach mode can be expressed as [7]

$$\nu = \gamma \cdot \left[H_i \cdot \left(H_i + 4\pi M_s \right) + \left(2\pi M_s \right)^2 \cdot \left(1 - e^{-2q_{\parallel} d} \right) \right]^{1/2} \tag{1}$$

with γ the gyromagnetic ratio, $4\pi M_s$ the saturation magnetization, $q_{\parallel}$ the in-plane wave vector, and d the dot thickness. H_i is the internal field, which is here defined as

$$H_i = H - H_d = H - N \cdot 4\pi M_s \tag{2}$$

with N the demagnetizing factor of the magnetic dots and H_d the demagnetizing field. Eq. (1) presumes a saturation of in-plane magnetization of the dots.

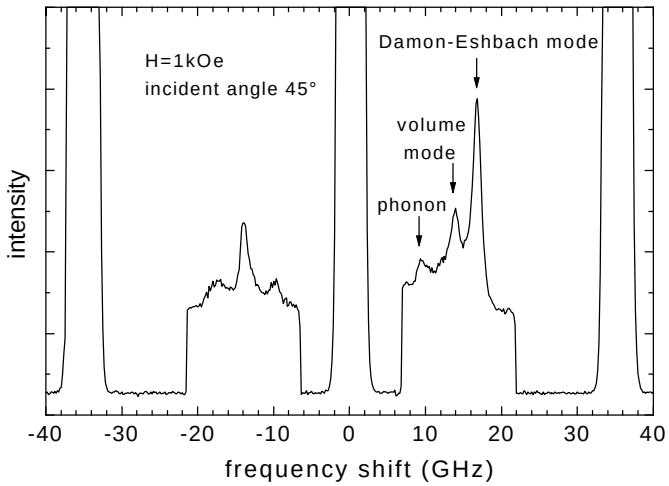

Fig. 1. Spin wave spectrum of a 2/4 µm sample of 500 Å thickness at an applied field of 1kOe at an angle of light incidence of 45°. At zero frequency the elastically scattered light, and at frequencies of ±(33–37) GHz the first ghost peaks are observed. In the region of interest ±(6.5–22) GHz the scan speed is reduced and thus the scattering intensity is increased. As indicated in the Figure the Damon-Eshbach mode, a standing spin wave (volume mode) and a surface phonon is observed.

Fig. 2 shows the observed dispersion curve of the Damon-Eshbach mode (squares) for the 2/2.2 µm sample as a function of the in-plane wave vector, $q_{\parallel}$. The solid line is a fit using Eq. (1) with the thickness d of the dots as a fit parameter. The fitted value of d = 940 Å is in very good agreement

with the nominal thickness of 1000 Å. No indications of a mode quantization due to the finite size of the dots, i.e., a lateral confinement of the spin wave modes, as reported for magnetic bars by *Gurney* et al. [2], or of spin wave zone folding effects as predicted by Kolodin et al. [10] have been observed for the investigated samples.

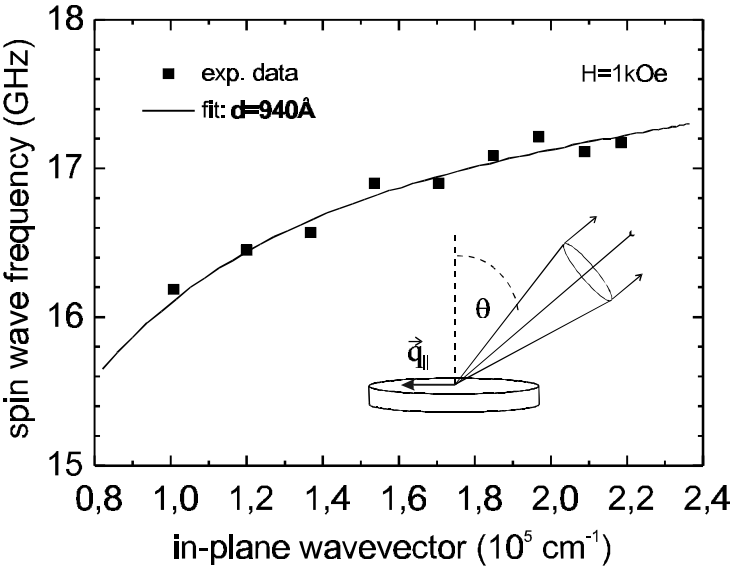

Fig. 2. Dispersion of the spin wave frequency for the 2/2.2 µm sample as a function of the in-plane wave vector, $q_{||}$. The scattering geometry is indicated in the inset. The squares are the experimental data and the solid line is a fit to the data.

We have investigated in detail the dependence of the spin wave frequencies on the strength of the external field [5,6]. Fig. 3 shows the results for the 1000 Å thick films. As obtained from the data displayed in Fig. 3 the spin wave frequencies are mostly sensitive to the dot diameter and to a much lesser degree to the dot separation. The solid lines are model calculations using Eq. (1) and calculating the demagnetizing factor, *N*, assuming spheroidally shaped dots with diameter *l* to thickness *d* ratios as indicated in the figure. A fairly good agreement between the measured and the calculated values is achieved for the data of spin wave frequencies larger than 14.5 GHz, where the dots are magnetically saturated. For smaller values, i.e., for $H < 1$ kOe for the $l = 0.5$ µm dots, and $H < 0.6$ kOe for the $l = 1.0$ µm dots, a breakdown of a uniform island magnetization is observed.

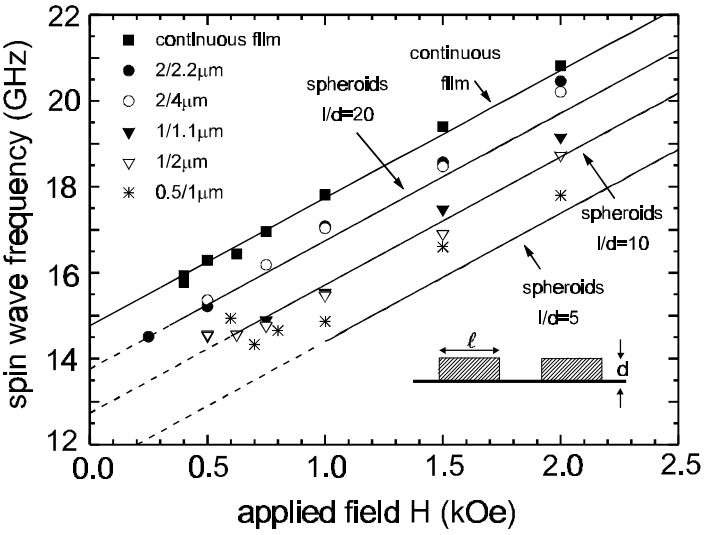

Fig. 3. Measured spin wave frequencies as a function of the strength of the applied external field, *H*. The symbols denote the measured data as indicated. The solid lines are fits to the data using aspect ratios of the spheroidal dot shapes as indicated in the Figure.

To clarify the problem of an in-plane interdot coupling, we measured the spin wave frequencies of the Damon-Eshbach mode as a function of the angle of the in-plane applied field, Φ_H, with respect to a reference [10]-direction of the lattice. Only for the smallest dot separations of 0.1 µm a fourfold

anisotropic behavior is found. This is displayed in Fig. 4 for the 1/1.1 μm and, for comparison, for the 1/2 μm lattices of the sample of 1000 Å thickness at an applied field of 1 kOe [11]. To determine quantitatively the anisotropy constant we use the free anisotropy energy expression

$$F = K^{(4)} \sin^2 \Phi \cdot \cos^2 \Phi \qquad (3)$$

with Φ the angle between the direction of magnetization with respect to the [10]-direction, and $K^{(4)}$ a fourfold in-plane anisotropy constant

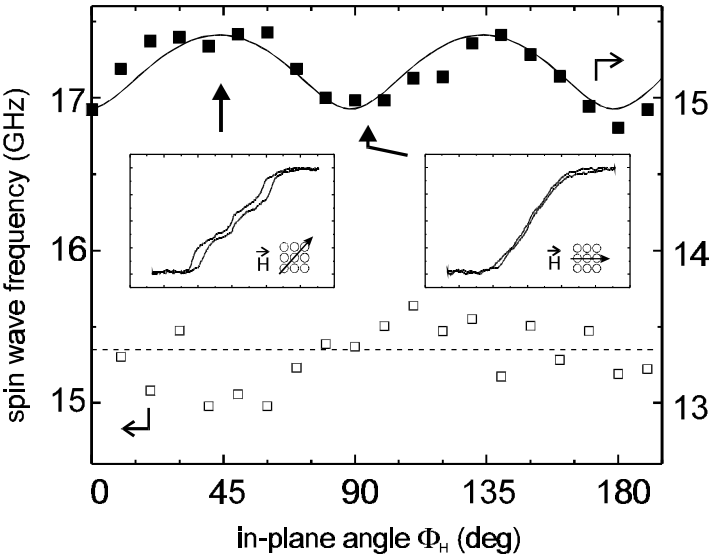

Fig. 4. Dependence of the spin wave frequencies on the in-plane direction of the applied field for the 1/1.1 μm (■) and, for comparison, for the 1/2 μm (□) dot lattices of 1000 Å thickness. The solid line is a fit for the data (see text). Kerr hysteresis loops of the 1/1.1 μm dot lattice are shown as insets with the applied field as indicated. Note the complicated magnetization reversal behavior of the 1/1.1 μm dot lattice for a field direction of 45°.

A model fit using Eq. (3) and a numerical procedure to calculate the spinwave frequencies [12] is displayed in Fig. 4 as a solid line for the 1/1.1 μm lattice. For both 1/1.1 μm samples with thicknesses of 500 Å and 1000 Å the anisotropy contribution $K^{(4)}$ was determined for several values of the applied magnetic field strength, H. The obtained results for $K^{(4)}$ are displayed for both thicknesses in Fig. 5 as a function of the reduced field H/H_d. $K^{(4)}$ decreases with increasing reduced field and saturates within the investigated field range at $K^{(4)} = -0.6 \cdot 10^5$ erg/cm^3, which corresponds to an effective anisotropy field $H_{ani} = 150$ Oe, at the same reduced field value of about $H/H_d = 5$. The data of both dot thicknesses fall onto one common curve within the error margins indicating that the coupling strength scales with the demagnetizing field.

The origin of this fourfold anisotropy can be understood as follows. Because of the large distance of 0.1 μm between the dots a direct exchange mechanism via conduction electrons or via electron tunneling can be excluded. The quasi-uniform demagnetization field, caused by the shape of the patterned area (1x1 mm^2 square) can not be responsible for the observed anisotropy. In fact, the film thickness/square length ratio is of the order of 10^{-4}. It corresponds to a demagnetizing field of about 1 Oe, which is much smaller than the observed value of 150 Oe. Moreover, since the quasi-uniform field strength should depend on the average magnetization of the lattice, the effect should be the same for 1/1.1 μm and the 2/2.2 μm lattices, which is not the case. A dipolar interaction of completely magnetized dots also cannot account for the observed anisotropy, because the corresponding dipolar energy can be expressed as a bilinear form of the components of the magnetization vector. Such an expression can only yield an uniaxial, but not a four-fold anisotropy contribution, since in a bilinear form the direction cosines appear quadratic in highest order and add to a constant if a fourfold symmetry is given. Therefore we propose that the fourfold anisotropy contribution is caused by a dipole-dipole interaction between residual unsaturated parts of the dots, because in this case the

energy cannot be expressed as a bilinear form. The large observed decrease of the coupling anisotropy constant with increasing field as well as the scaling of the anisotropy with the reduced field corroborates this assumption. The anisotropic coupling is still observed for field values larger than the demagnetizing field, H_d. However, due to the non-ellipsoidal form of the dots and due to surface magnetic anisotropies acting on the dot boundaries, which cannot be characterized in more detail in the present study, it is likely that the non-saturated parts can persist up to fairly high fields.

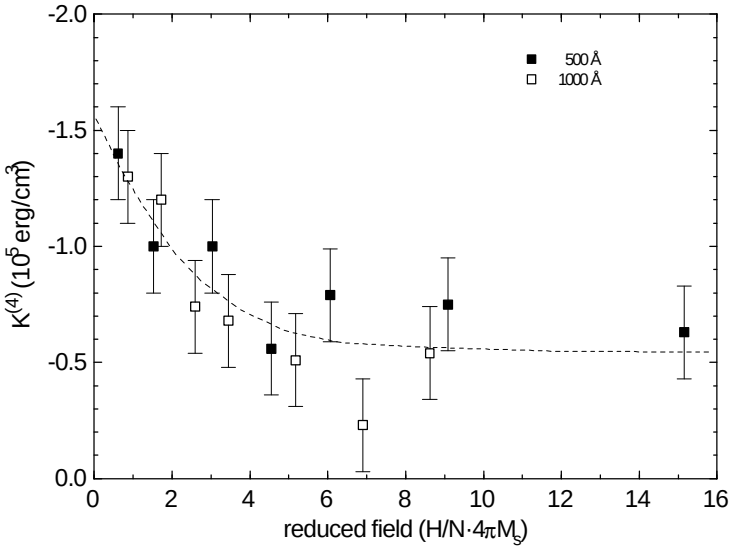

Fig. 5. Fourfold anisotropy constant, $K^{(4)}$, for the 1/1.1 μm lattices of 500 Å and 1000 Å thickness as a function of the reduced field ($H/N \cdot 4\pi M_s$). The dashed line serves as a guide to the eyes.

To study more precisely the static magnetization behavior Kerr measurements were carried out. Only for the lattices with the smallest dot separation of 0.1 μm a fourfold in-plane anisotropy in the loop shapes is found. For comparison Kerr loops of the 1/1.1 μm lattice of 1000 Å thickness are shown as insets in Fig. 4, with the magnetic field, H, applied along the [10]- and the [11]-direction. In comparison, the loop shape of the 1/1.1 μm lattice along the [10]-direction is very similar to the loop shapes of the 1/2 μm lattices for all field directions. In contrary the loop shape of the 1/1.1 μm lattice with H along the [11]-direction, i.e. the easy direction of $K^{(4)}$ as determined by BLS, is rather complex. Similar loop shapes have been obtained by Smyth et al. as a function of the interdot separation but the magnetization reversal process is not yet understood [1,3]. Since these loop shapes exhibit a higher zero-field susceptibility, they also indicate that the [11]-direction is the easy axis. Another result is that the saturation field H_s decreases with decreasing dot separation, which can be well understood as a result of an increasing film coverage. For the 1/1.1 μm and the 1/2 μm lattices the values of H_s are (620±50) Oe and (780±50) Oe, respectively. This result is qualitatively in agreement with the BLS data, showing the spin wave frequencies of the 1/1.1 μm lattice lying slightly above the frequencies of the 1/2 μm indicating smaller demagnetizing fields for the sample with lower spacings. A direct proof of a coupling of stray fields due to the presence of a common magnetic substructure of the dots is yielded by magnetic force microscopy (MFM). The measurements were performed at zero applied field. MFM-images of the 1/1.1 μm and the 1/2 μm lattices of 500 Å thickness are shown in Fig. 6. For both lattices a heterogeneous magnetic structure is clearly recognizable, which seems to be totally disordered for the large separation of 1 μm. For the 1/1.1 μm lattice a regular pattern of the domain walls can be seen, which are aligned crosslike along the [10]-direction, consistent with a closed domain structure. This is evidence for a separation dependent dipolar coupling of the domains, which is only effective for separations of the order of 0.1 μm.

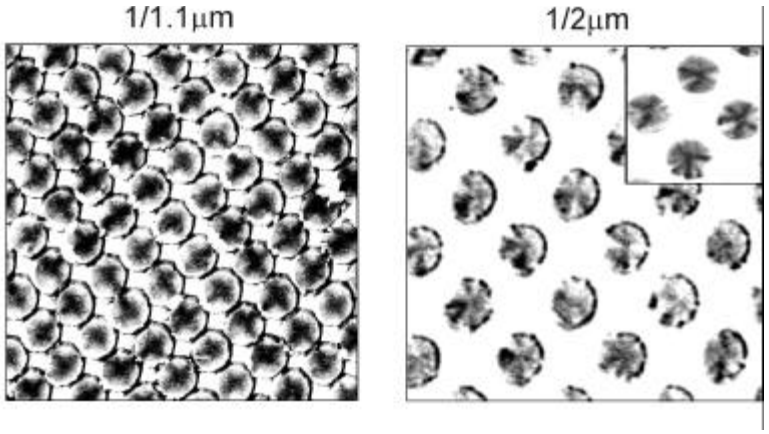

Fig. 6. MFM images of the 1/1.1 μm and 1/2 μm samples of 500 Å dot thickness. Note the crosslike order of domain walls along the [10]-direction for the 1/1.1 μm lattice in contrary to their irregular orientation for the 1/2 μm lattice. For clarity an inset with a better resolution is shown for the 1/2 μm sample.

In summary, using spin waves as a tool to investigate magnetic properties in dot arrays, the most striking effect is the demagnetizing effect of the individual dots. It should be noted that the large dependence on the demagnetizing factor is due to the fact, that the spin wave wavelength of ≈2000 Å is comparable to the island sizes. A breakdown of the uniform island magnetization can be easily observed in the spin wave spectra. From fitting the spin wave dispersion curves the dot thicknesses obtained agree with the nominal thicknesses. We have found clear evidence for a fourfold in-plane anisotropic coupling of magnetic micron dots, most probably mediated by stray fields of non-saturated parts of the dots. The anisotropy strength is of the order of 10^5 erg/cm^3. Since the coupling has been found only for the smallest dot separation of 0.1 μm investigations of further reduced dot separations are required. For a full description of the spin wave mode dispersion in these patterned structures model calculations taking in detail the size and the shapes of the islands into account are greatly needed.

References

[1] J.F. Smyth, S. Schultz, D. Kern, H. Schmidt, D. Yee, J. Appl. Phys. **63**, 4237, (1988).
[2] B.A. Gurney, P. Baumgart, V. Speriosu, R. Fontana, A. Patlac, T. Logan, P. Humbert, Digest of the International Conference on Magnetic Films and Surfaces, Glasgow, (1991).
[3] J.F. Smyth, S. Schultz, D.R. Fredkin, D.P. Kern, S.A. Rishton, H. Schmid, M. Cali, T.R. Koehler, J. Appl. Phys. **69**, 5262 (1991).
[4] A. Maeda, M. Kume, T. Ogura, K. Kukori, T. Yamada, M. Nishikawa, Y. Harada, J. Appl. Phys. **76**, 6667 (1994).
[5] B. Hillebrands, C. Mathieu, M. Bauer, S.O. Demokritov,B. Bartenlian, C. Chappert, D. Decanini, F. Rousseaux, F. Carcenac, J. Appl. Phys. **81** (8) 4993 (1997)
[6] C. Mathieu, C. Hartmann, M. Bauer, O. Büttner, S. Riedling, B. Roos, S.O. Demokritov, B. Hillebrands, B. Bartenlian, C. Chappert, D. Decanini, F. Rousseaux, E. Cambril, A. Müller, B. Hoffmann, and U. Hartmann, Appl. Phys. Lett. **70** 2912 (1997).
[7] R.W. Damon, J.R. Eshbach, J. Phys. Chem. Solids **19**, 308 (1961).
[8] F. Rousseaux, D. Decanini, F. Carcenac, E. Cambril, M.F. Ravet, C. Chappert, N. Bardou, B. Bartenlian, P. Veillet, J. Vac. Technol. B **13**, 2787 (1995).
[9] Equations (1, 2) describe in good approximation the observed gross feature of the shape effects also in presence of anisotropies, since the anisotropy contributions are small.
[10] P.A. Kolodin, B. Hillebrands, J. Magn. Magn. Mater. **161**, 199 (1996).
[11] The data of the 1/2 μm sample show compared to the 1/1.1 μm sample a larger scatter in the data due to the smaller light scattering cross section caused by the lower magnetic coverage, but the data indicate clearly, that no significant fourfold anisotropy contribution is present in this sample.
[11] B. Hillebrands, Phys. Rev. B **44**, 530 (1990).

6.9 Spin wave quantization in mesoscopic permalloy bar structures

C. Mathieu, J. Jorzick, S.O. Demokritov, and B. Hillebrands[1]

Our previous studies on structured magnetic films revealed many very interesting physical aspects, in particular an anisotropic coupling of magnetic dots forming a square lattice (see Sect. 6.8) [1-3]. The phenomenon of a quantization of spin waves due to a confinement within the magnetic structures or due to periodicity effects could not be detected in the dot arrays, probably due to the geometry of these samples. Therefore we chose the more appropriate geometry of magnetic bar arrays for a search of quantization effects.

The samples consist of a 270 Å thick permalloy ($Ni_{81}Fe_{19}$) film deposited in UHV onto a Si (111) substrate. Patterning was done by X-ray lithography at the LURE synchrotron in France and a lift-off technique. Two patterned areas with periodic arrays of bars with widths of 2 µm and periodicities of 2.5 µm and 4 µm were investigated. A continuous film of the same thickness served for reference. The arrays were patterned over an area of 500×500 μm^2.

In a thin ferromagnetic film with the direction of magnetization perpendicular to the spin wave wavevector and within the film plane, two types of spin wave modes exist, the dipolar dominated, so-called Damon-Eshbach mode and the exchange dominated standing spin waves. The latter modes are not further considered here, since they depend only on the film thickness due to a quantization of the perpendicular spin wave wavevector component, but not on the pattern parameters.

With the bars perpendicular to the spin wave wavevector of the Damon-Eshbach mode parallel to the film plane, $q_{\|}$, two additional quantization conditions might appear. First, due to the finite bar width, a standing-wave (Fabry-Perot) condition should be fulfilled:

$$q_{\|} = 2\pi / \lambda = n\pi / w, \quad n = 1,2,3... \tag{1}$$

Second, due to the periodic arrangement of the bars with the periodicity Λ, a folding of the dispersion curve and the formation of gaps at discrete $q_{\|}$-values might appear:

$$q_{\|} = m\pi / \Lambda, \quad m = 1,2,3... \tag{2}$$

The Brillouin light scattering experiments were performed in backscattering geometry using a computer controlled tandem Fabry-Perot interferometer. The in-plane wave vector, $q_{\|}=(4\pi/\lambda_{Laser})\cdot\sin\theta$, of the tested spin waves was varied by changing the angle of light incidence, θ. A field of 500 Oe was applied in the film plane and perpendicular to the spin wavevector.

With θ_n the angle of incidence, at which the quantization condition Eq. (1) is fulfilled, we obtain:

$$\sin\theta_n = \frac{q_{\|}(n)\lambda_{Laser}}{4\pi} = \frac{\lambda_{Laser}}{4w}\cdot n \tag{3}$$

Fig. 1 shows a Brillouin light scattering spectrum for a wavevector of $q_{\|}=2.1\cdot10^4$ cm^{-1} for the sample with Λ=2.5 µm. Near ±7 and ±8 GHz two distinct magnetic excitations are observed on each side of the spectrum with a Stokes/anti-Stokes asymmetry of the scattered light intensity characteristic for Damon-Eshbach modes. By varying the wavevector $q_{\|}$, the spin wave dispersion of Fig. 2 is obtained. Shown are the data for Λ=4 µm (top), 2.5 µm (middle) and, for reference, for a continuous

[1] in collaboration with B. Bartenlian and C. Chappert, IEF, Université Paris-Sud, France, D. Decanini, F. Rousseaux, and E. Cambril L2M, Bagneux, France

film. The patterned films show two distinct, dispersionless modes for $q_{\|} < q_{\|}^0 \approx 3 \cdot 10^4$ cm^{-1}, corresponding to $q_{\|}^0 = 2\pi/w$. For the sample with the large bar separation, a splitting into two modes is observed also near $2\,q_{\|}^0$, $3\,q_{\|}^0$ and $4\,q_{\|}^0$. These splittings are not clearly observed for Λ=2.5 µm (Fig. 2, middle). For $q_{\|}$ parallel to the bars no splitting is observed.

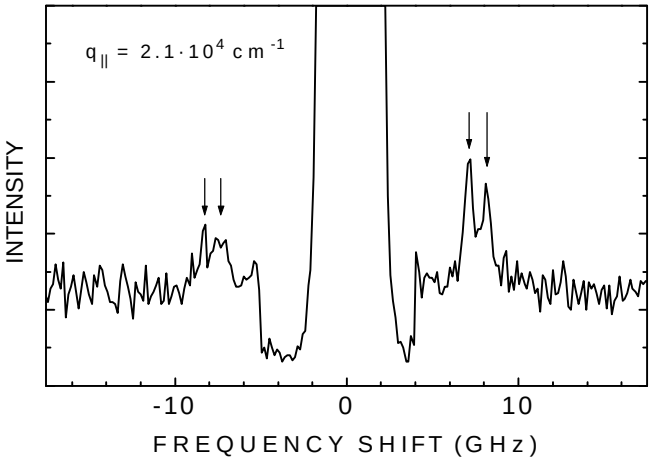

Fig. 1. Spin wave spectrum of the sample with Λ= 2.5 µm. The applied field was 0.5 kOe. The arrows indicate the mode splitting of about 1 GHz. In the region (5 ... 4) GHz the light intensity was reduced to avoid an overload of the detector.

From comparing the data for L=4 µm and for L=2.5 µm the following conclusions can be drawn: i) The quantization of the spin-wave excitations in two dispersionless modes for $q_{\|} \leq q_{\|}^0$ is caused by the finite width of the bars. The fact that the frequency difference between the two modes is independent of L indicates a single bar effect and excludes, that the quantization is due to the periodic bar arrangement. ii) The separation $\Delta q_{\|} = q_{\|}^0$ between the wavevector values, at which additional splittings into two modes are observed, is compatible with Eq. (1) assuming that n is only taking even numbers. iii) Within the experimental resolution there is no indication for anomalies in the obtained dispersion curves caused by zone folding effects due to the periodicity L of the bar patterns.

The observed mode splitting of $q_{\|}^0 \approx 1$ GHz is not consistent with a lateral standing spin wave excitation caused by a pinning of the spins at the side walls of the bars, for which a calculation, based on a quantization of the parallel wavevector as expressed in Eq. (1), yielded a frequency splitting of 20 MHz, much smaller than the experimentally obtained value. There exist some calculations of eigenmodes of magnetic bars but they are not appropriate for this problem due to the deviating square cross section of the bars [4]. In our case the aspect ratio of the bars is roughly 75. Although the bars could only be coupled by their weak dipolar stray fields since the translation symmetry is broken in one of both in-plane film directions due to the patterning, the obtained dispersion of the dipolar spin wave mode resembles fairly close by the dispersion of a continuous film. This might not be surprising for large wavevectors, where the bar width is large compared to the spin wave wavelength. In the region of small wavevectors, where the integer n (see Eq. 1) counting the number of half wavelengths fitting into a bar is a small number, the observed dispersion can be understood as follows: The intrinsic excitations of the bar array are the eigenmodes of the individual bars. In the small wavevector regime the dispersion of a continuous film splits up in neighboring levels of these dispersionless eigenexcitations of the bars. The obtained dispersion can be understood as a mapping of the dispersion of an infinite film onto the eigenmodes of the bars. For larger wavevectors the separation of the eigenmodes becomes smaller and probably the width of the modes increases, resulting in a smearing out of the modes, and thus resembling more closely the monotonous dispersion of a continuous film.

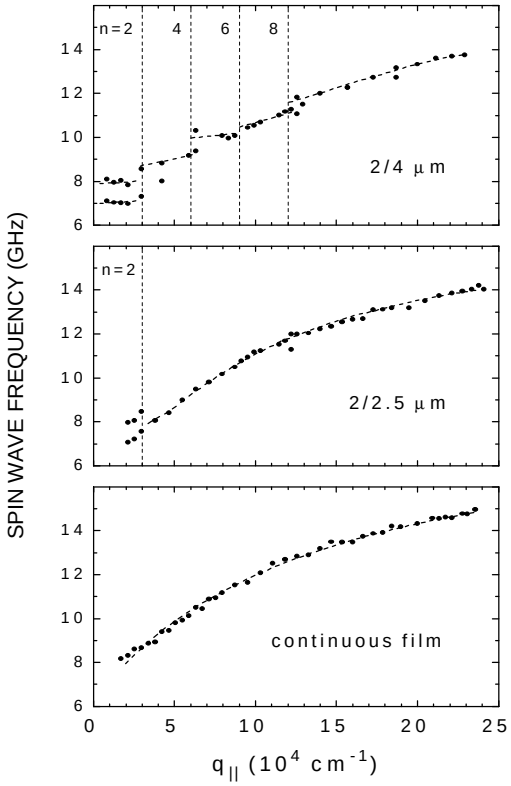

Fig. 2. Obtained spin wave dispersion curve for a bar separation of 2 µm (upper part) and 0.5 µm (middle part) and for continuous film as a reference (lower part).

In summary we have observed mode quantization effects in periodic arrays of magnetic bars. The two modes observed for small wavevectors are identified as eigenmodes of the bars. For larger wavevectors a quasi-continuous spin wave dispersion resembling rather closely the dispersion of a continuous film is obtained, with mode splittings at discrete values of the wavevector. Further experimental investigations are in progress to clarify more deeply the nature of the observed phenomena. An appropriate theoretical modeling of these observed phenomena is also needed.

A full report is published in [5].

References

[1] C. Mathieu, C. Hartmann, M. Bauer, O. Büttner, S. Riedling, B. Roos, S.O. Demokritov, B. Hillebrands, B. Bartenlian, C. Chappert, D. Decanini, F. Rousseaux, E. Cambril, A. Müller, B. Hoffmann, U. Hartmann, Appl. Phys. Lett. **70**, 2912 (1997).

[2] B. Hillebrands, C. Mathieu, C. Hartmann, M. Bauer, O. Büttner, S. Riedling, B. Roos, S.O. Demokritov, B. Bartenlian, C. Chappert, D. Decanini, F. Rousseaux, E. Cambril, A. Müller, B. Hoffmann, U. Hartmann, J. Magn. Magn. Mater., in press.

[3] B. Hillebrands, C. Mathieu, M. Bauer, S.O. Demokritov, B. Bartenlian, C. Chappert, D. Decanini, F. Rousseaux, F. Carcenac, J. Appl. Phys. **81**, 4993 (1997).

[4] T.M. Sharon, A.A. Maradudin, J. Chem. Phys. Solids **38**, 972 (1977).

[5] C. Mathieu, C. Hartmann, J. Jorzick, S.O. Demokritov, B. Hillebrands, B. Bartenlian, C. Chappert, D. Decanini, F. Rousseaux and E. Cambril, submitted to Phys. Rev. B.

6.10 Parametric excitations of spin waves

O. Büttner, C. Mathieu, and B. Hillebrands[1]

In the last years the parametric excitation of spin waves has become of growing interest because of its application in the amplification of the amplitude of solitons traveling in thin magnetic films [1-2]. A typical setup for soliton amplification experiments consists of an input antenna where a short microwave pulse excites a soliton which is detected at an output antenna several mm away from the input antenna. Between input and output antenna there is an additional antenna where a microwave field at twice the frequency of the input antenna amplifies the soliton amplitude.

The parametric excitation of spin waves is a three magnon process in which the magnon, which is excited by the microwave field, decays into two magnons at the half frequency and with opposite k-vectors. This process has a well defined power threshold above that the number of excited spin waves grows exponentially with the microwave input power. The effect is well known for spin waves in thin films in homogeneous microwave fields created by, e.g., a microwave cavity [3-8]. Subject of our study is the determination of the influence of an inhomogeneous microwave field, like it is created by a microstrip antenna, on the parametric excitation.

We used Brillouin light scattering spectroscopy (BLS) to investigate the spin waves parametrically excited by a microstrip antenna. The BLS technique has a high sensitivity to spin waves, in particular to those at large k-vectors, and it has a high spatial resolution of about 50 µm. To determine the spin wave distribution near the input antenna, which is mounted on an opaque substrate, we performed the measurements in backscattering geometry. The sample is a 2 mm wide Yttrium Iron Garnet (YIG) film with a thickness of 5 µm. It was mounted onto a microstrip antenna with a length of 2.5 mm and a width of 35 µm. To avoid heating of the sample by the microwaves, the microwave signal was modulated by a frequency of 40kHz which leads to an average input power of ~1/10 of the peak power.

A typical BLS spectrum for parametric excitation is shown in Fig. 1. The microwave frequency was 10.9 GHz. The input peak power was ≈900 mW. The peak in the BLS count rate at 5,4 GHz which

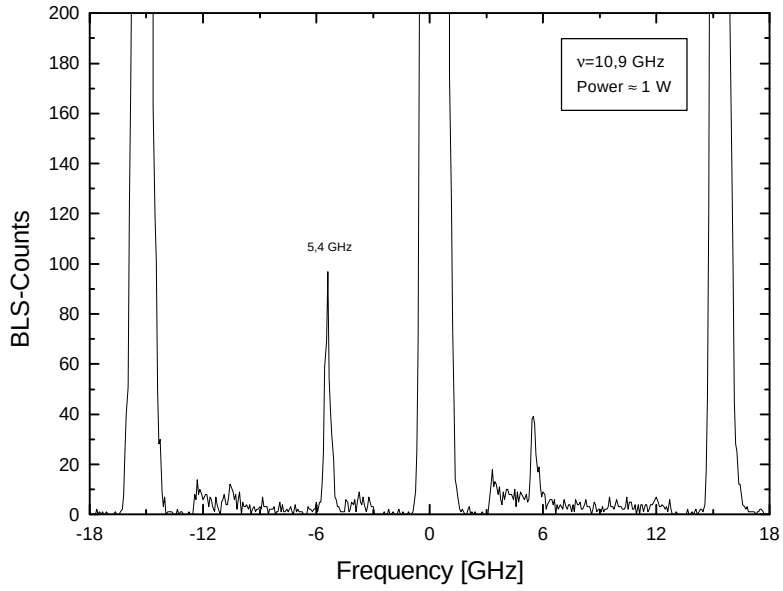

Fig. 1. A typical BLS-Spectrum for a parametrically excited spin wave using a microstrip antenna for the excitation. The microwave frequency is 10.9 GHz, the input peak power is ≈900 mW. The peaks at -5.4 GHz and 5.4 GHz are the Stokes and the anti-Stokes signals of the parametrically excited spin waves in the film.

is half the microwave frequency is clearly seen in the spectrum.

To find the threshold for the parametric excitation we increased the input power of the microwaves and measured the count rate of the inelastically scattered light. The result of these measurements is shown in Fig. 2. The exponential growth of the signal starts at ≈725 mW and no saturation is observed in the accessible power range.

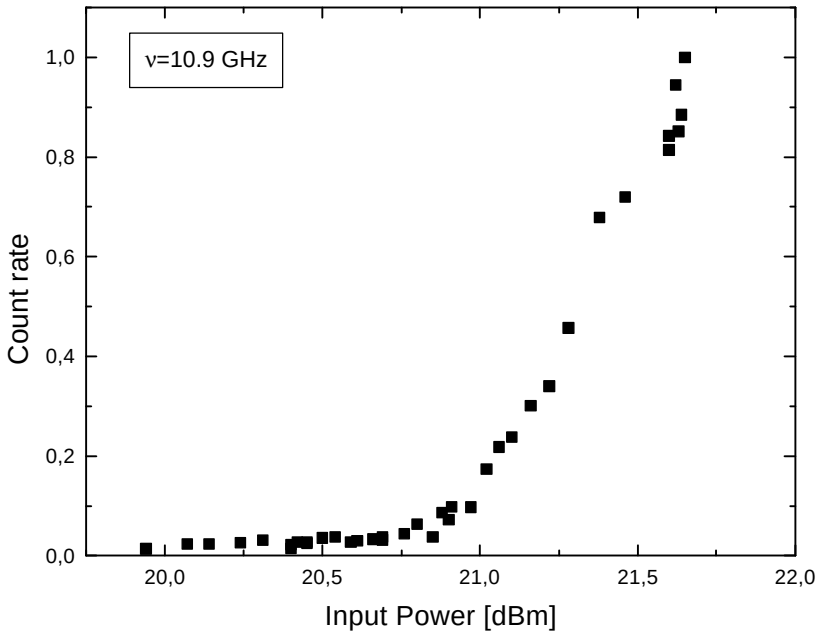

Fig. 2. BLS count rate versus input power for the parametric excitation experiment. The exponential growth starts at 725 mW and continues up to the maximum power of the microwave input signal.

To find out the propagation properties of the spin waves we scanned along the sample and determined the BLS signal. However a significant spin wave signal could only be detected directly at the input antenna. The reason for that is yet not clear. A possible explanation is that the k-vector is very high which leads to a low group velocity of the spin waves. The waves are exponentially attenuated due to damping with a factor of $\exp(-\omega_r/v_g)$ where ω_r describes the damping, which is independent of the k-vector, and v_g is the group velocity. Due to this exponential factor the waves with lower group velocity decay very fast so that the waves with high k-vectors cannot propagate in the sample. Another reason could be that the spin waves propagate parallel to the antenna. This could not be examined in the experiment because of the size of the sample which had a width of only 2 mm which is smaller than the length of the input antenna. The study of the propagation in a sample larger than the antenna will be subject of forthcoming experiments.

References

[1] B.A. Kalinikos, N.G. Kovshikov, M.P. Kostylev and H. Benner, Pis'ma ZhETF **64**, 160 (1996).
[2] A.V. Bagada, G.A. Melkov, A.A. Serga and A.N. Slavin, J. Appl. Phys. **81**, 5081 (1997).
[3] W. Wettling, W.D. Wilber, P. Kabos and C.E. Patton, Phys. Rev. Lett. **51**, 1680 (1983).
[4] W.D. Wilber, J.G. Booth, C.E. Patton, G. Srinivasan and R.W. Cross, J. Appl. Phys **64**, 5477 (1988).
[5] P. Kabos, G. Wiese and C.E. Patton, Phys. Rev. Lett. **72**, 2093 (1994).
[6] P. Kabos, C.E. Patton, G. Wiese, A.D. Sullins, E.S. Wright and L. Chen, J. Appl. Phys. **80**, 3962 (1996).
[7] G. Wiese, P. Kabos and C.E. Patton, J. Appl. Phys. **74**, 1218 (1993).
[8] G. Wiese, P. Kabos and C.E. Patton, Phys. Rev. B **51**, 15085 (1995).

[1]in collaboration with M. Kostylev and B. Kalinikos, Electrotechnical University St Petersburg, Russia.

6.11 Nonlinear spin wave propagation in YIG and Bi-substituted YIG films

O. Büttner, M. Bauer, S.O. Demokritov, and B. Hillebrands[1]

Spin waves propagating in thin magnetic films are a very good model system to investigate the linear and nonlinear wave dynamics. A wide range of effects can be observed [1]. The normal setup for an experiment to examine the spin wave behavior is a microwave network in which the spin waves in the films are excited by a microwave input antenna and detected by an output antenna, so that it is possible to measure the reflected and the transmitted microwave signal. The disadvantage of this method is, that it is not possible to get information about the spin wave propagation properties between the antennas. To measure the two dimensional spin wave amplitude distribution in a magnetic film we used the Brillouin light scattering (BLS) technique which is an excellent technique for such measurements due to its high spatial resolution of about 50 µm and its high dynamic range of >50 dB [2].

The behavior of a spin wave beam in a thin magnetic field can be described by a nonlinear Schrödinger equation (NSE):

$$i\left(\frac{\partial\varphi}{\partial t}+V_g\frac{\partial\varphi}{\partial z}\right)+\frac{1}{2}D\frac{\partial^2\varphi}{\partial z^2}+S\frac{\partial^2\varphi}{\partial y^2}-N|\varphi|^2\varphi=-i\omega_r\varphi$$

$$V_g=\frac{\partial\omega_k}{\partial k_z},\quad D=\frac{\partial^2\omega_k}{\partial k_z^2},\quad S=\frac{\partial\omega_k}{\partial k_y^2},\quad N=\frac{\partial\omega_k}{\partial|\varphi|^2}$$

where φ is the dimensionless amplitude of the wave beam, V_g is the group velocity, D is the dispersion coefficient, S is the diffraction coefficient, N is the non-linear parameter and ω_r describes the dissipation. ω_k is the dispersion relation.

For magnetostatic backward volume waves (MSBVW) the dispersion coefficient (D) and the diffraction coefficient (S) are positive, while the non-linear parameter (N) is negative, so that the Lighthill criteria [3] for longitudinal modulational instabilities, $ND<0$, and for transversal modulational instabilities, $NS<0$, are both fulfilled. This leads in the case of the absence of dissipation to a wave collapse at a wave-beam amplitude threshold $|\varphi_{th}|$. With dissipation there is no such a collapse, but the wave beam should be focused at some distance from the antenna.

In our experiments we studied the evolution of a quasi-plane wave front initial beam in a $Lu_{2.04}Bi_{0.96}Fe_5O_{12}$ (BIG) film which was epitaxially grown onto a single crystalline (111)-oriented gallium gadolinium garnet (GGG) substrate. The size is 2 × 10 mm^2 and the thickness is 1.5µm. The sample was mounted on a standard delay-line-structure with input and output antennas (width r=35µm, length W=2.5 mm) separated by a distance of 8 mm and connected to a network analyzer (Fig. 1).

[1]in collaboration with S. Sure, H. Dötsch, Universität Osnabrück, Germany, A.N. Salvin, Oakland University, Rochester, Michigan, U.S.A., V. Grimalsky, Yu. Rapoport, Kiev State University, Ukraine, and P. A. Kolodin, St. Petersburg Electrotechnical University, Russia.

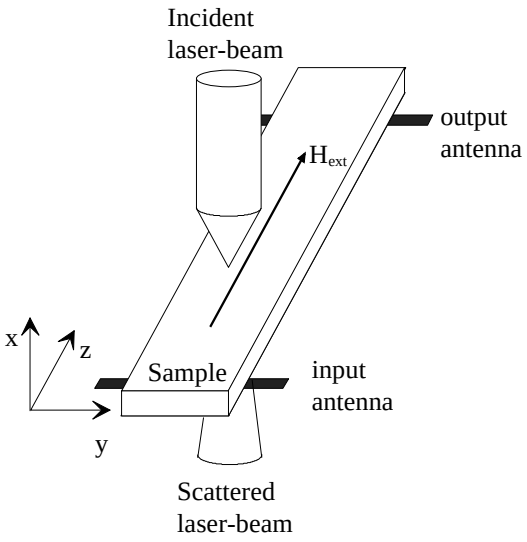

Fig. 1. Experimental setup. The antennas are connected to a network analyzer. The sample is scanned in the *y*- and *z*-direction.

The results of the measurements are shown in Fig. 2. The mesh used for the two dimensional scan along the sample was 0.1 mm along y and 0.5 mm along z. The input power is indicated below each panel. The numbers above the panels indicate the value of maximum spin wave

a)

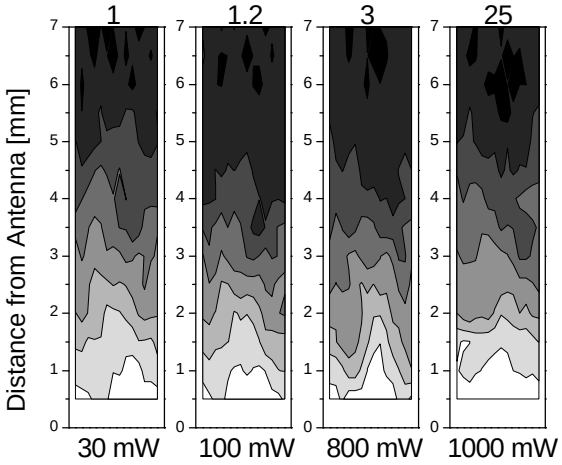

Fig. 2. Measured MSBVW intensity distribution in a ferrimagnetic BIG-film at the microwave input powers as indicated at the bottom of the figure. The origin of the z-axis denotes the position of the input antenna. The frame indicates the width of the sample of 2 mm. Bright/dark intensities indicate high/low spin-wave intensities. The numbers above the panels indicate the value of the maximum spin wave count rate for each measurement, which is a measure of the spin wave intensity. a) Raw data without attenuation correction, b) attenuation corrected data. At a power of 800 mW the self-focusing of the wave beam appears at a distance of 1.5 mm from the input antenna.

b)

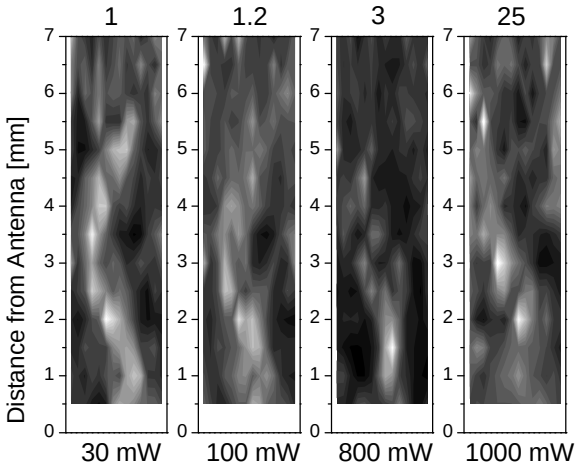

count rate for each measurement normalized to the value of smallest microwave intensity, which is a measure of the spin wave intensity. Bright/dark intensities in the picture indicate high/low spin-wave intensities. The raw data are shown in Fig. 2a. The mode profile clearly shows a narrowing at a power of 800 mW. Despite the complicated intensity profile in the yz-plane and its dependence on the input power the average spin-wave attenuation shows a simple exponential decay proportional to $e^{-\kappa z}$, where κ is the damping parameter and z is the distance from the antenna, as is shown in Fig. 3. Here the logarithm of the integrated intensity of the spin wave modes as a function of the distance to the input antenna is shown. As can be seen, the behavior is the same for all power levels. The straight line is a fit to the data and yields the attenuation parameter of κ = 76.3 dB/cm. This constant exponential decay can be used to improve the contrast of the raw data. By plotting $a \cdot e^{\kappa z}$, where a is the measured spin wave amplitude, one can avoid the large changes in the plotted values of the amplitude. This was done in Fig. 2b. A pronounced feature of the plot is a sharp, high intensity spot at a distance of 1.5 mm from the input antenna for an input power of 800 mW which we interpret as evidence for the self-focusing effect. Another feature of all measurements is the snake like structure which appears for all input powers and which will be discussed from the theoretical point of view in Sect. 6.12.

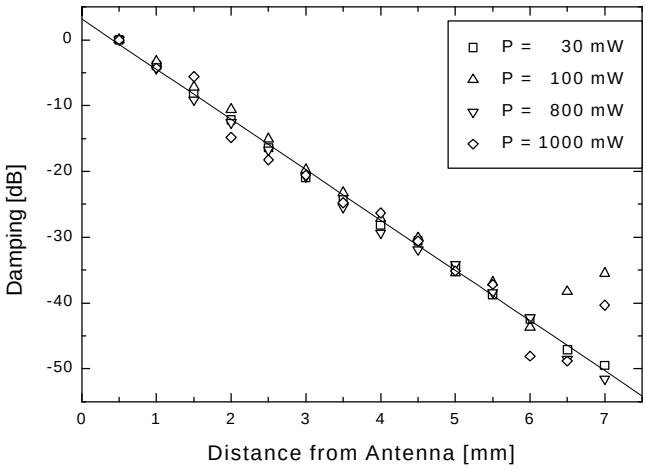

Fig. 3. Integrated modes of the spin wave intensity as a function of the distance from the antenna. The attenuation parameter obtained from a fit (full line) is κ= 76.3 dB/cm

References

[1] see, e.g, *Nonlinear Phenomena and Chaos in Magnetic Materials*, P.E. Wigen (ed.) (World Scientific, Singapore, 1994).

[2] M. Bauer, C. Mathieu, S.O. Demokritov, B. Hillebrands, P.A. Kolodin, S. Sure, H. Dötsch, V. Grimalsky, Yu. Rapoport and A.N. Slavin, Phys. Rev. B **56**, R8483 (1997).

[3] M.J. Lighthill, J. Inst. Math. Appl. **1**, 269 (1965).

6.12 Snake-like spin wave propagation in magnetic waveguides

O. Büttner, M. Bauer, S.O. Demokritov, M. Kostylev, and B. Hillebrands[1]

In Sec. 6.11 we reported on measurements of the two-dimensional intensity distribution of spin-wave excitations in a $Lu_{2.04}Bi_{0.96}Fe_5O_{12}$ film. To simulate the behavior of the spin wave beam we numerically solved the nonlinear Schrödinger equation for different initial conditions [1,2]. At first we used a sinusoidal initial distribution which describes the excitation of a single spin wave mode with one k-vector in the y-direction. This leads to the results shown in Fig. 1. The numbers below the panels indicate the spin wave amplitude relative to the threshold amplitude where the nonlinear effects balance the attenuation. The upper panels show the calculations with the exponential attenuation. The lower panels are corrected for the attenuation as described in Sec. 6.11. The evolution from the linear beam without any changes in the beam shape to the self focusing can clearly be seen. The panel on the right hand side shows a chaotic multifoci distribution at very high input powers.

Comparing the results from the numerical calculations with the measured data, the correspondance is very good for the development of the self focusing. The distance of the focus point from the antenna of 1.5 mm for $|\varphi/\varphi_{th}|^2 = 5$ is in accordance with the measured distance for 800 mW input power.

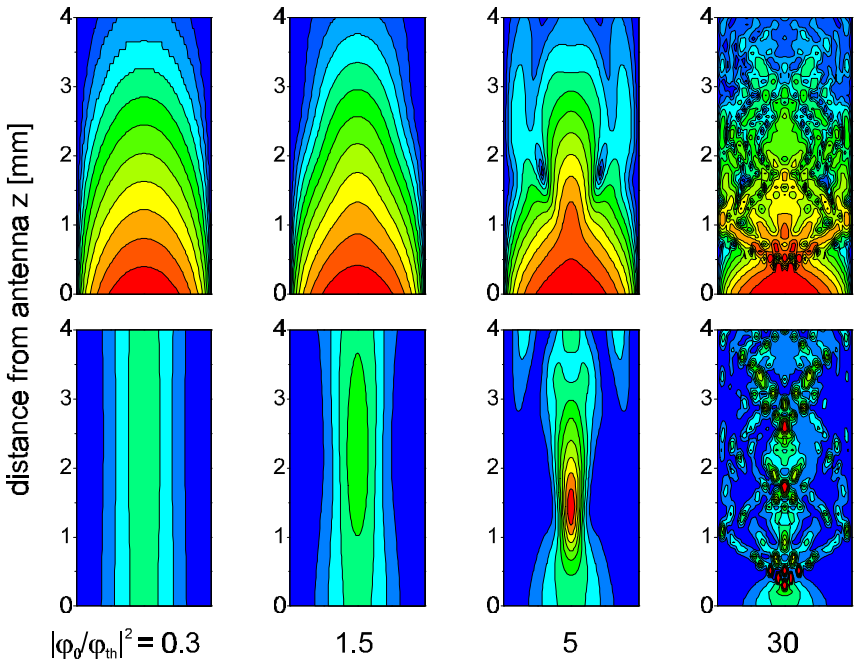

Fig. 1. Numerically calculated stationary distribution of the spin wave intensity. Upper panels show the amplitude distribution normalized to the maximum intensity of the initial (z = 0) beam intensity distribution in a logarithmic scale. Lower panels show the distribution in a linear scale.

Despite the good correspondence between measurement and simulation for the formation of the self focusing, the second striking feature of the measurements, the snake like structure which appears for all power levels, is not included in the results of the numerical calculations. Therefore we reformulated the numerical calculation taking the waveguide nature of our sample explicitely into account. The width of the sample of 2 mm can cause the excitation of not only the first wave mode in the y-direction but also the excitation of higher harmonics. Since the modulus of the k-vector is still the same for all modes, the z-component of the k-vector is different for the different higher-order modes.

[1]in collaboration with A.N. Slavin, Oakland University, Rochester, Michigan, U.S.A., and Yu. Rapoport, Kiev State University, Ukraine.

This leads to different phase velocities of the modes and therefore to an interference pattern along the sample.

With this new approach we simulated the intensity distribution using the ansatz

$$j\ (y, z=0) = A\left\{\sin\frac{\pi y}{b} + \frac{1}{3}\sin\frac{2\pi y}{b}\right\}$$

with b the width of the waveguide. The results are displayed in Fig. 2. The left panel shows the linear case for low input powers and the right panel shows the case for high input powers. As can be clearly seen, the development of the self-focusing is still included in the results and in addition the snake like structure is now correctly contained in the simulation.

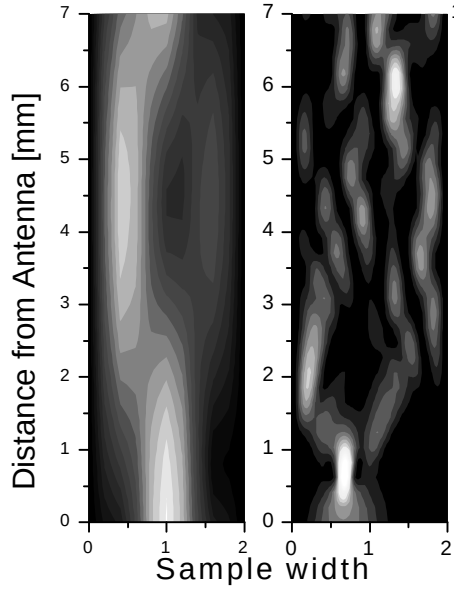

Fig. 2. The left panel shows the results of the analytical model for small spin wave intensities corresponding to the linear regime. The right panel shows the result of our numerical calculations for $|\varphi_0/\varphi_{th}|=5$. The origin of the *z*-axis is the position of the input antenna.

References

[1] M. Bauer, C. Mathieu, S.O. Demokritov, B. Hillebrands, P.A. Kolodin, S. Sure, H. Dötsch, V. Grimalsky, Yu. Rapoport and A.N. Slavin, Phys. Rev. B **56**, R8483 (1997).

[2] O. Büttner, M. Bauer, C. Mathieu, S.O. Demokritov, B. Hillebrands, P.A. Kolodin, M.P. Kostylev, S. Sure, H. Dötsch, V. Grimalsky, Yu. Rapoport and A.N. Slavin, submitted to IEEE Trans. Mag.

6.13 Spin waves and magnetic anisotropy in ultrathin (111)-oriented cubic films

G. Gubbiotti[#°], G. Carlotti[#], and B. Hillebrands[°]

[#]*Unita' INFM- Dipartimento di Fisica dell'Universita', Via Pascoli, 06100 Perugia, Italy*
[°]*Fachbereich Physik, Universität Kaiserslautern, Erwin-Schrödinger-Str. 56, 65663 Kaiserslautern*

The study of spin waves in magnetic films with cubic symmetry has shown to be very useful for determining magnetic anisotropy constants. For the (111) orientation spin-wave frequency calculations have not been presented so far probably due to the more complicated algebra involved and due to the lack of experimental data. Recently an appreciable directional in-plane dependence of the spin-wave frequency has been observed by Brillouin light scattering (BLS) in ultrathin Ni films [1]. The aim of this work, which is the result of a collaboration between the Universities of Perugia (Italy) and of Kaiserslautern, is to fill the gap existing in the literature concerning the characteristics of the spin-wave spectrum of thin and ultrathin magnetic films with (111) orientation. It is important to note that the (111) plane is unique among the principal planes in a cubic crystal in the sense that the variation of the first non-vanishing order bulk anisotropy contribution, as a function of the direction of the magnetization, is greatly reduced as compared to other planes. A consequence of this is that a data fit of the spin-wave frequency as a function of the in-plane propagation direction yields precise measurements of the interface in-plane anisotropy constant.

The spin-wave frequency is calculated making use of the full numerical procedure in the dipole-exchange [2] regime for an in-plane magnetized Ni film and including both (111) magneto-crystalline

$$E_{ani} = K_1\left\{\frac{1}{3}\cos^4\theta + \frac{1}{4}\sin^4\theta - \frac{\sqrt{2}}{3}\sin^3\theta\cos\theta\cos(3\phi)\right\} \quad (1)$$

and interface anisotropy

$$E_{inter} = -k_s\cos^2\theta - k_p\frac{\sqrt{2}}{3}\sin^3\theta\cos\theta\cos(3\phi) \quad (2)$$

Contributions.

For the following simulations, the applied field is 1 kOe and we have always kept the volume anisotropy constant to the fixed value of K_1 = -5.1×10^4 erg/cm^3 and the out-of-plane anisotropy constant to k_s = 0.375 erg/cm^2. The values of the other magnetic parameters are reported in Ref. [1].

Fig. 1 shows the spin-wave dispersion of the Damon-Eshbach mode as a function of the angle ϕ for the principal planes of a 200 Å thick Ni film with the in-plane interface anisotropy constant k_p set to zero. Therefore the directional dependence of the spin-wave frequency is only caused by the magnetocrystalline bulk anisotropy in the simulations. Maxima in the spin-wave frequencies indicate easy directions of the magnetization. For the (111)-oriented film, the frequency shows a six-fold periodicity, which reflects the in-plane layer symmetry, and the amplitude of the frequency oscillation is greatly reduced with respect to those with respect to the (100)- and the (110)-oriented films. For these last two orientations, the four-fold and two-fold angular periodicity result from the symmetry of the bulk anisotropy fields. Our calculations indicate that the experimental determination of the in-plane anisotropy constants from the spin-wave frequency dispersion is very difficult for thick (111)-Ni films since the frequency dispersion with the in-plane angle is comparable with or lower than the typical Brillouin scattering resolution (≅0.3 GHz).

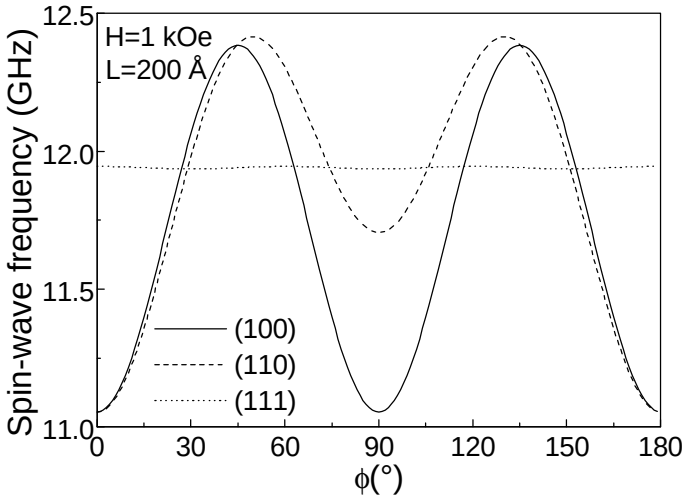

Fig. 1. Spin-wave frequencies for the principal planes of a cubic crystal as a function of the angle ϕ for an applied magnetic field of 1.0 kOe. The in-plane anisotropy is set to zero on both film interfaces.

This type of measurements becomes more feasible in the case of ultrathin films since the interface anisotropy constant k_p which is of 3-fold rotational symmetry, and converted into an effective volume anisotropy field, yields a large contribution to the angular dispersion of the spin-wave frequency. To illustrate this aspect the calculated angular dispersion of the spin-wave frequency for a (111)-oriented 200 Å thick Ni film is compared in Fig. 2 with that of Ni films of lower thicknesses (100 Å and 50 Å).

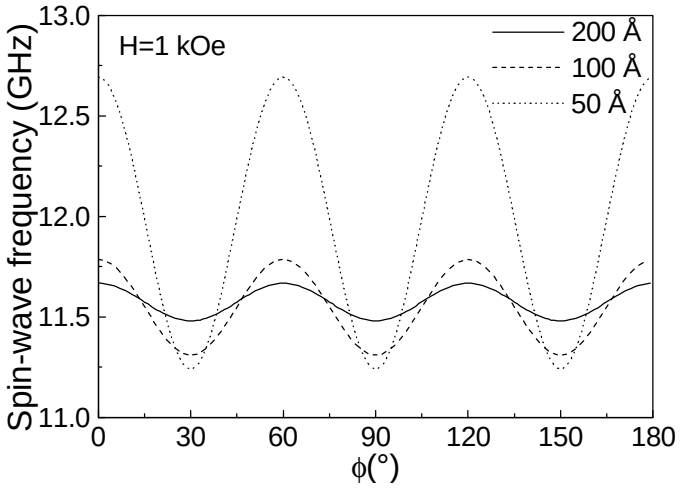

Fig. 2. Spin-wave frequencies for (111)-oriented cubic crystal as a function of the angle ϕ for film thickness of 200 Å, 100 Å and 50 Å.

The curves are calculated assuming the interface anisotropy constants k_p = 0.15 erg/cm^2 and k_s = 0.375 erg/cm^2. The peak-to-peak frequency amplitude, which essentially depends on k_p, increases from about 0.2 GHz, for the thick films, to approximatively 1.4 GHz, for the a 50 Å thick Ni film. This is within the range of sensitivity of a typical BLS experiment.

As a general comment on the results obtained, we notice that the frequency variation versus the angle ϕ in thick films is rather small, but this variation increases in ultrathin films because of the greater contribution given by the in-plane anisotropy energy which is converted into an effective volume anisotropy.

References

[1] G. Gubbiotti, G. Carlotti, G. Socino, F. D'Orazio, F. Lucari, R. Bernardini, and M. De Crescenzi, Phys. Rev. B **56**, 11073 (1997).

[2] G. Gubbiotti, G. Carlotti, and B. Hillebrands, submitted to J. Phys. C.

6.14 Elasticity of hard amorphous carbon films

V. Wiehn, P. Cortina, K. Jung and B. Hillebrands

One of the aims of this project is to establish the Brillouin light scattering spectroscopy as a method to characterize the elastic properties of hard and superhard thin films. During the last year thin films of amorphous hydrogenated carbon have been prepared by plasma beam coating. The plasma beam source used to produce the films is shown in Fig. 1.

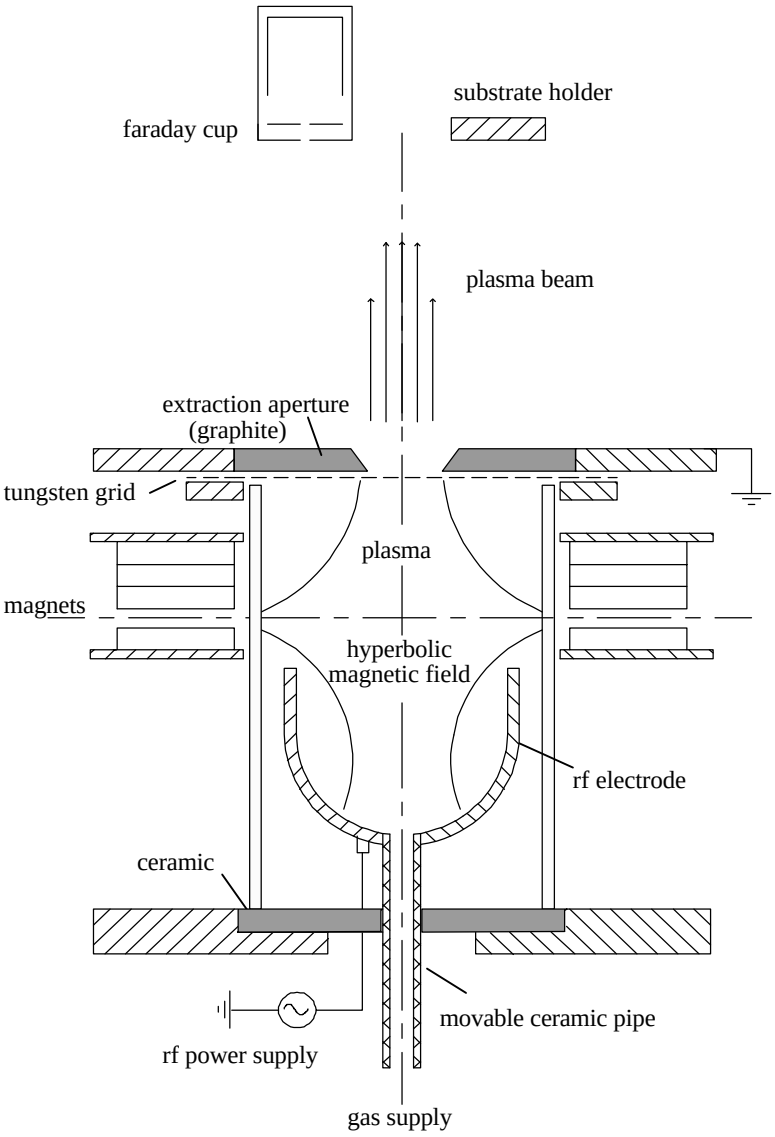

Fig.1 Schematic diagram of the plasma beam source

In a 13.56 MHz discharge C_2H_2 is effectively ionized. A hyperbolically shaped magnetic field helps to concentrate the plasma in the middle of the discharge zone. Thus the gas pressure can be chosen rather low with about $4 \cdot 10^{-3}$ mbar leading to a low rate of chemical gas reactions. Therefore and because of the stability of C_2H_2 against dissociation by electron impact mainly $C_2H_2^+$ and C_2H^+ ions leave the discharge region through a tungsten grid. The Faraday cup allows, if it is positioned in the beam axis, to control the beam intensity and the ion beam distribution. The ion energy per carbon atom, which is well defined within 10%, can be varied between 60 eV and a few hundred eV by changing the position of the powered electrode. The ion flux intensity of the rather homogeneous plasma beam is about 0,5 mA/cm^2. Because of the quasi-neutrality of the beam also insulating materials can be coated.On the substrate, hit by the quasi-neutral plasma beam, a diamond-like amorphous carbon film is growing which contains 20% to 40% hydrogen depending on the energy of the ions. In a rather narrow ion energy range around 100 eV per carbon atom a metastable carbon film is produced which contains a high percentage of tetrahedrically bonded carbon atoms. The impact of the medium energy ions leading to a soft subsurface implantation has the effect that the material is substantially densified. The amorphous carbon network tends to undergo a transformation from the low density graphite-like to the high density diamond-like configuration. The so-called ta-C:H material is very hard. The films may have only thicknesses of a few hundred

nm because of the high internal stress of the growing material. Thicker films are destroying themselves by cracking and delaminating.

The ion energy of the impinging $C_2H_2^+$ ions and the deposition temperature are the essential parameters determining the ratio of diamond-like to graphite-like bonded carbon atoms. Superhard films containing mainly tetrahedrically bonded amorphous carbon grow at room temperature and the ion energies have to be about 96 eV per carbon atom. Most of the films studied until now have not been very hard because the Brillouin light scattering signals of first samples of superhard thin films have been very weak. The reason for the small signal could be that the very high stress of these films leads to a damping of the surface waves caused by inhomogeneities of the material with respect to the elastic properties on the 100 nm length scale.

The elastic properties of the prepared superhard thin films are determined by Brillouin light scattering of green laser light from thermically excited surface phonons. By measuring the dispersion relations of the perpendicularly polarized Rayleigh and Sezawa waves all relevant components of the elastic tensor can be determined. Especially the moduli of stress and of shear can be deduced from the experimental data.

Fig. 2 shows the dispersion curves taken from the Brillouin light spectra for one of the specimen. The dotted lines show theoretical dispersion curves fitted to the experimental data. From the fit the four components of the elastic tensor given in the figure can be extracted.

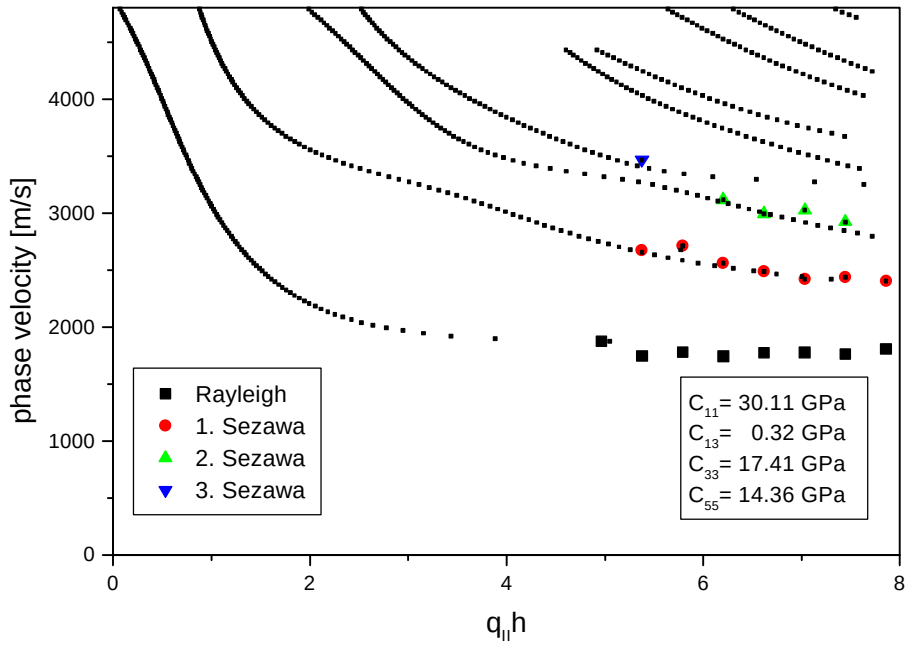

Fig. 2: Dispersion curves of the Rayleigh- and several Sezawa-modes of a 340 nm thick a-C:H film. The deposition parameters are listed in the main text. The small dots are a fit to the data

The material has been grown on silicon by impact of $C_2H_2^+$ ions of 120 eV per carbon constituent at a deposition temperature of 450°C. On these conditions the material is partly nanocristalline. Hardness and stress are reduced relative to the films deposited at room temperature, resulting in rather low values of the various components of the elasticity tensor.

6.15 Absence of elastic anomalies for Co/Ni superlattices with oscillatory transport

C. Hartmann, C. Mathieu, and B. Hillebrands[1]

Recently observed oscillations of the resistivity ρ and the anisotropic magnetoresistance in Co/Ni superlattices as a function of the superlattice periodicity Λ [1] caused us to search for a correlation between these oscillations and anomalies in the elastic constants. The origin for the oscillations of the resistivity is described by an electron localization model, in which *d* electrons are assumed to be localized within the superlattice structure, giving rise to strong *s*-*d* scattering, when the *d* states cross the Fermi level with changing Λ. Because the electronic structure, in particular the density of states at the Fermi level, is expected to influence the elastic constants, we investigated the elastic constants as a function of the superlattice periodicity.

The elastic constants were determined by Brillouin light scattering from surface and film acoustic phonons, the so-called Rayleigh and Sezawa modes. The Rayleigh mode is a long-wavelength acoustic surface excitation, the Sezawa modes are higher order acoustic phonons, only localized in a film (i.e. the Co/Ni superlattice) deposited onto a substrate. From the sound velocities of these modes the elastic constants are determined.

An anomaly in any of the elastic constants should therefore manifest itself in a modification of the dispersion curves of the Rayleigh and/or Sezawa modes.

The Co/Ni (fcc/fcc) superlattices were grown in San Diego by molecular beam epitaxy (MBE) onto single-crystalline (110)-oriented sapphire substrates with (111)-texture of the Co and Ni films. The superlattice periodicity Λ was chosen to be between 20 Å and 59 Å while the thickness of the samples was nearly held constant at about 1000 Å. The measurements were performed in backscattering geometry using a computer controlled tandem Fabry-Perot interferometer and light of a 514.5 nm Ar^+ ion laser. The Rayleigh mode and the first Sezawa mode were clearly identified.

Since Λ was small compared to the wavelengths of the investigated modes, an effective medium model for the elastic constants could be used in good approximation. The sound velocity dispersion curves as a function of the product of the in-plane wave vector $q_{||}$ and the sample thickness *h* are displayed is Fig. 1 for two samples with extremal values in the resistivity.

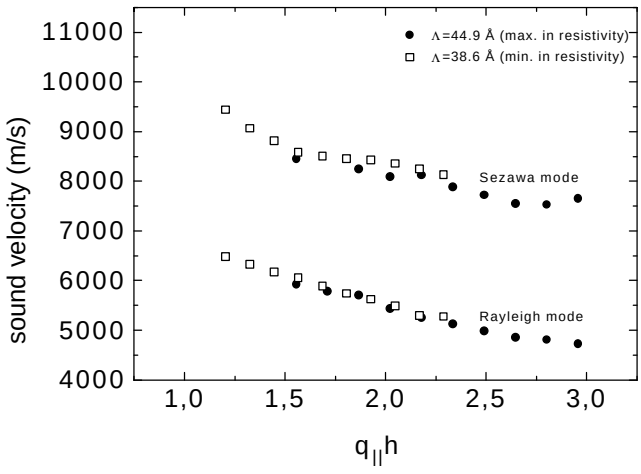

Fig. 1. Experimental sound velocity dispersion curves as a function of the product of the wavevector, $q_{||}$, and the sample thickness *h*, of the acoustic modes (Rayleigh and first Sezawa mode) for two samples with extremal values in the resistivity.

[1] in collaboration with S. Kim and I.K. Schuller, University of San Diego, U.S.A.

Both the Rayleigh and Sezawa mode decrease in velocity with increasing $q_{\parallel} \cdot h$. The dispersions of the two samples overlap within a large region of $q_{\parallel} \cdot h$ indicating the elastic properties to be very similar. Taking into account any differences in the thicknesses of the samples, the values of the sound velocities have been determined for a common $q_{\parallel} \cdot h$ value of $q_{\parallel} \cdot h = 2.3$. These data are shown in Fig. 2 together with the resistivity data.

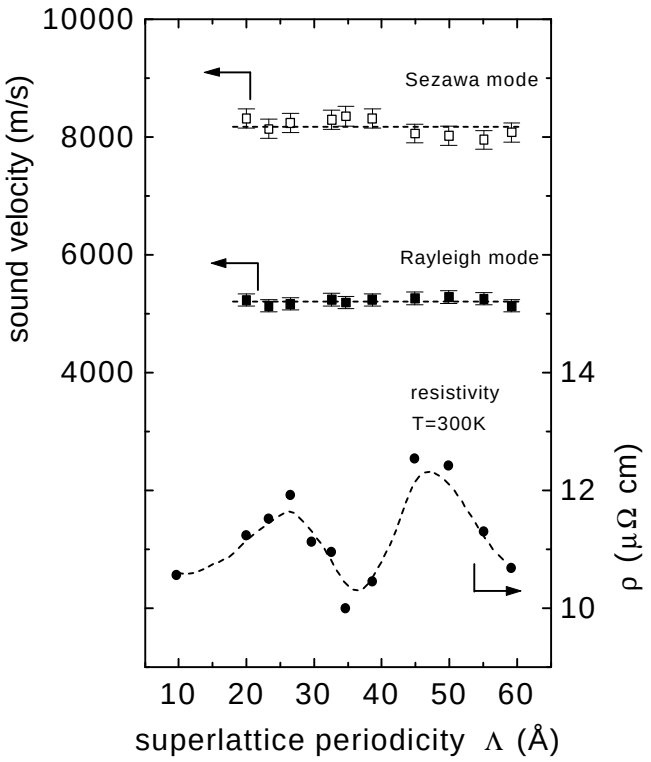

Fig. 2. Obtained sound velocities of the Rayleigh and the Sezawa mode for a common value of $q_{\parallel} \cdot h = 2.3$ as a function of the superlattice periodicity, Λ. The dashed lines are linear fits to the data. For reference the resistivity data are shown as well.

The main result is, that within an experimental error of ±2%, all sound velocities lie at constant values, i. e., both the Rayleigh and the Sezawa mode are independent of the superlattice periodicity Λ.

In conclusion, no correlation with the resistivity $\rho(\Lambda)$ was found. Most probably this implies that the contribution of the density of states near the Fermi level to the elastic properties is negligible.

A full report is published in [2].

References

[1] Sihong Kim, D. Lederman, J. M. Gallego and I. K. Schuller, Phys. Rev. B **54**, 5291 (1996).
[2] C. Hartmann, C. Mathieu, B. Hillebrands, Sihong Kim and Ivan K. Schuller, Phys. Rev. B **55** 14074 (1997).

Chapter 7: Publications (1996-1997)

1. *Domain structure and anisotropy of exchange coupled Co/Cr/Fe multilayers,* T. Kleinefeld, M. Figge, K. Theis-Bröhl, R. Scheidt, T. Zeidler, C. Mathieu, B. Hillebrands, J. Appl. Phys. **79,** 4531 (1996).

2. *Ferromagnetism above room temperature in Mn-Si-C- alloy films, M. Gajdzik, C. Sürgers*, M. Kelemen, B. Hillebrands and H. v. Löhneysen, Appl. Phys. Lett. **68**, 3189 (1996).

3. *Suppression of the magnetocrystalline bulk anisotropy in thin epitaxial Co (110) films on Cu(110)*, B. Hillebrands, J. Fassbender, R. Jungblut, G. Güntherodt, D.J. Roberts, G.A. Gehring, Phys. Rev. B **53**, 10548 (1996).

4. *Magnetic exchange coupling effects in asymmetric trilayer structures of MBE grown Co/Cr/Fe*, K. Theis-Bröhl, R. Scheidt, T. Zeidler, F. Schreiber, H. Zabel, T. Mathieu, C. Mathieu, B. Hillebrands, Phys. Rev. B **53**, 11613 (1996).

5. *Antiferromagnetic interlayer coupling in epitaxial Fe/EuS(100) bilayers,* U. Rücker, S.O. Demokritov, R.R. Arens, P. Grünberg, J. Magn. Magn. Mater. **156**, 269 (1996).

6. *Structural relaxation and magnetic anisotropies in Co/Cu(001) films,* W. Weber, R.A. Bischof, R. Allenspach, C.H. Back, J. Faßbender, U. May, B. Schirmer, R.M. Jungblut, G. Güntherodt, B. Hillebrands, Phys. Rev. B **54**, 4075 (1996).

7. *Spin-wave propagation across periodically corrugated thin metallic ferromagnetic films*, P.A. Kolodin, B. Hillebrands, J. Magn. Magn. Mater. **161**, 199 (1996).

8. *Enhancement of the Curie temperature of epitaxial EuS(100) films, caused by growth dislocations*, S.O. Demokritov, U. Richter, P. Grünberg, J. Magn. Magn. Mater. **163**, 21 (1996).

9. *Magnetic properties of ultrathin epitaxial Co films studied by Brillouin light scattering*, B. Hillebrands, J. Faßbender, P. Krams, C. Mathieu, G. Güntherodt, R. Jungblut, Il Vuoto, Scienza e Tecnologia **25**, 24 (1997).

10. *Interface anisotropy and magnetization reversal in epitaxial Fe(001)/Pd double layers,* S.O. Demokritov, C. Mathieu, M. Bauer, S. Riedling, O. Büttner, H. de Gronckel, B. Hillebrands, J. Magn. Magn. Mater. **165**, 496 (1997).

11. *Brillouin light scattering investigations of structured permalloy films,* B. Hillebrands, C. Mathieu, M. Bauer, S.O. Demokritov, J. Appl. Phys. **81**, 4993 (1997).

12. *Anisotropic magnetic coupling of permalloy micron dots forming a square lattice*, C. Mathieu, C. Hartmann, M. Bauer, O. Büttner, S. Riedling, B. Roos, S.O. Demokrotiv, B. Hillebrands, B. Bartenlian, C. Chappert, D. Decanini, F. Rousseaux, E. Cambril, A. Müller, B. Hoffmann, U. Hartmann, Appl. Phys. Lett. **70**, 2912 (1997).

13. *Absence of elastic anomalies for Co/Ni superlattices with oscillatory transport*, C. Hartmann, C. Mathieu, S. Kim, I. Schuller, B. Hillebrands, Phys. Rev. B **55**, 14074 (1997).

14. *Wall energy and wall thickness of exchange-coupled rare-earth transition-metal triple layer stacks*, D. Raasch, C. Mathieu, J. Appl. Phys. **82**, 1 (1997).

15. *Propagation of linear and nonlinear spin wave excitations in YIG and LuBiFeO films studied by space resolved Brillouin light scattering (extended abstract)*, M. Bauer, C. Mathieu, S.O. Demokritov, B. Hillebrands, P.A. Kolodin, S. Sure, H. Dötsch, A.N. Slavin, J. Appl. Phys. **81**, 3971 (1997).

16. *Static and dynamic properties of patterned magnetic permalloy films*, B. Hillebrands, C. Mathieu, C. Hartmann, M. Bauer, O. Büttner, S. Riedling, B. Roos, S.O. Demokritov, B. Bartenlian, C. Chappert, D. Decanini, F. Rousseaux, E. Cambril, A. Müller, B. Hoffmann, U. Hartmann, J. Magn. Magn. Mater, in press.

17. *Direct observation of two-dimensional self-focusing and initial stages of a wave collapse for spin waves in magnetic films*, M. Bauer, C. Mathieu, S.O. Demokritov, P.A. Kolodin, S. Sure, H. Dötsch, A.N. Slavin, B. Hillebrands, Phys. Rev. B **56** R8483 (1997).

18. *Biquadratic interlayer coupling in layered magnetic systems*, S.O. Demokritov, J. Phys. D, in press.

19. *Brillouin light scattering investigations of exchange biased (110)-oriented NiFe/FeMn bilayers*, C. Mathieu, M. Bauer, B. Hillebrands, J. Faßbender, G. Güntherodt, R. Jungblut, J. Kohlhepp, A. Reinders, J. Appl. Phys, in press.

20. *Dynamic finite size effects in magnetic bar arrays*, C. Mathieu, C. Hartmann, J. Jorzick, S.O. Demokritov, B. Hillebrands, B. Bartenlian, C. Chappert, D. Decanini, F. Rousseaux, E. Cambril, submitted to Phys. Rev. B, Brief Reports.

21. *Correlation between structure and magnetic anisotropies of Co on Cu(110)*, J. Fassbender, G. Güntherodt, C. Mathieu, B. Hillebrands, R. Jungblut, J. Kohlhepp, M.T. Johnson, D.J. Roberts, G.A. Gehring, submitted to Phys. Rev. B.

22. *Mode beating of spin wave beams in ferrimagnetic $Lu_{2.04}Bi_{0.96}Fe_5O_{12}$ films*, O. Büttner, M. Bauer, C. Mathieu, S.O. Demokritov, B. Hillebrands, P.A. Kolodin, M.P. Kostylev, S. Sure, H. Dötsch. V. Grimalsky, Yu Rapoport, A.N. Slavin, submitted to IEEE Trans. Magn.

23. *Spin waves and magnetic anisotropy in ultrathin (111)-oriented cubic films*, G. Gubbiotti, G. Carlotti and B. Hillebrands, submitted to J. Phys. C.

24. B. Hillebrands, *Brillouin light scattering from layered magnetic structures*, Light Scattering in Solids VII, Springer Series in Applied Physics, M. Cardona, G. Güntherodt (eds.), submitted.

Conferences:

Invited talks:

CAMST, Topical Meeting on Magnetic Nanostructures, Bristol, April 1996

First Toyota Workshop on Information Storage Materials, Brüssel, April 1997

European Workshop on Surface Brillouin Spectroscopy, Oxford, April 1997

Other conference contributions:

1 contribution:	Drei-Königs-Treffen Oberflächenmagnetismus, Physikzentrum Bad Honnef, January 1996
6 contributions:	Frühjahrstagung der DPG, Regensburg, March 1996
1 contribution:	SFB 166 Workshop, April 1996
1 contribution:	E-MRS-Spring Meeting, Straßburg, June 1996
3 contributions:	41st Annual Conference of Magnetism and Magnetic Materials, Atlanta (USA), November 1996
4 contributions:	Frühjahrstagung DPG, Münster, March 1997
1 contribution:	MRS-Spring Meeting, San Francisco, April 1997
1 contribution:	c-BN-Expertentreffen auf der Reichenau, June 1997
1 contribution:	D-A-CH-Kolloquium ’97, Altlengbach, October 1997

Invited colloquia and seminars:

B. Hillebrands:

Freie Universität Berlin, January 1996

University of Ferrara, Italy, October 1996

University of Perugia, Italy, October 1996

Universität Regensburg, January 1997

Universität des Saarlandes, Saarbrücken, February 1997

MPI für Mikrostrukturforschung, Halle, March 1997

University of Perth, Australia, August 1997

Charles University Prague, Czech Republic, September 1997

Technical University Ostrava, Czech Republic, September 1997

Siemens AG, Erlangen, November 1997

S.O. Demokritov:

St. Petersburg University, St. Petersburg, May 1996

IBM Almaden Research Center, San Jose, USA, March 1997

University of California, Irvine, USA, April 1997

Technische Universität Darmstadt, November 1997